JCTC Journal of Chemical Theory and Computation

pubs.acs.org/JCTC Article

ADT: A Generalized Algorithm and Program for Beyond Born−Oppenheimer Equations of "*N*" Dimensional Sub-Hilbert Space

Koushik Naskar,[¶] Soumya Mukherjee,[¶] Bijit Mukherjee, Satyam Ravi, Saikat Mukherjee, Subhankar Sardar, and Satrajit Adhikari*

Cite This: *J. Chem. Theory Comput.* 2020, 16, 1666−1680 Read Online

ACCESS | Metrics & More | Article Recommendations | Supporting Information

ABSTRACT: The major bottleneck of first principle based beyond Born−Oppenheimer (BBO) treatment originates from large number and complicated expressions of adiabatic to diabatic transformation (ADT) equations for higher dimensional sub-Hilbert spaces. In order to overcome such shortcoming, we develop a generalized algorithm, "ADT" to generate the nonadiabatic equations through symbolic manipulation and to construct highly accurate diabatic surfaces for molecular processes involving excited electronic states. It is noteworthy to mention that the nonadiabatic coupling terms (NACTs) often become singular (removable) at degenerate point(s) or along a seam in the nuclear configuration space (CS) and thereby, a unitary transformation is required to convert the kinetically coupled (adiabatic) Hamiltonian to a potentially (diabatic) one to avoid such singularity(ies). The "ADT" program can be efficiently used to (a) formulate analytic functional forms of differential equations for ADT angles and diabatic potential energy matrix and (b) solve the set of coupled differential equations numerically to evaluate ADT angles, residue due to singularity(ies), ADT matrices, and finally, diabatic potential energy surfaces (PESs). For the numerical case, user can directly provide *ab initio* data (adiabatic PESs and NACTs) as input files to this software or can generate those input files through in-built python codes interfacing MOLPRO followed by ADT calculation. In order to establish the workability of our program package, we selectively choose six realistic molecular species, namely, NO_2 radical, H_3^+, F + H_2, NO_3 radical, $C_6H_6^+$ radical cation, and 1,3,5-$C_6H_3F_3^+$ radical cation, where two, three, five and six electronic states exhibit profound nonadiabatic interactions and are employed to compute diabatic PESs by using *ab initio* calculated adiabatic PESs and NACTs. The "ADT" package released under the GNU General Public License v3.0 (GPLv3) is available at https://github.com/AdhikariLAB/ADT-Program and also as the Supporting Information of this article.

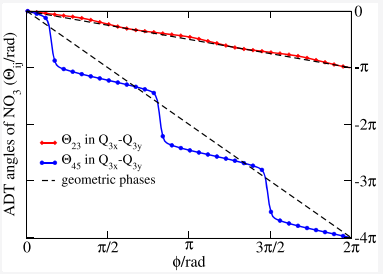

1. INTRODUCTION

The familiar theoretical framework of Born−Oppenheimer (BO) approximation[1,2] breaks down in several molecular and reactive systems due to the presence of significant coupling between electronic and nuclear motion. In other words, the most obvious origin of this failure is due to the significant contribution of nonadiabatic interactions between ground and the excited electronic states, which are frequently encountered in various natural processes, like chemical reaction, photosynthesis, vision etc. Nonadiabatic coupling terms (NACTs), a major outcome of the BO treatment, play a pivotal role in many chemical processes, specially at the degenerate or near-degenerate points/seams in the potential energy surfaces (PESs), where the removable components of NACTs could be singular according to Hellmann−Feynman theorem.[3,4] In order to produce correct spectral information on a molecule or to extract the dynamical features of a chemical reaction, the contribution of excited states must be gracefully included during the investigation even for a ground state treatment of a molecular process.[5−13]

In the early sixties, Longuet-Higgins pointed out sign inversion phenomenon of BO eigenfunctions[14] while encircling a point of degeneracy in the nuclear configuration space (CS) and this was corrected by multiplying a complex phase factor in an *ad hoc* manner.[15] Alternatively, Mead and Truhlar overcome this deficiency by including a vector potential in the nuclear kinetic energy operator.[16] Due to singular nature of removable (longitudinal) part of NACTs at the degenerate points/seams in the CS, an unitary transformation can be employed for hiding out singularity(ies) of NACTs in the form of potential coupling terms in the diabatic Hamiltonian. Hobey and McLachlan[17] first used the theoretical treatment of adiabatic to diabatic transformation (ADT) for a single degree of freedom to remove the coupling terms from adiabatic Schrödinger equation (SE), which, later on, was implemented by F. T. Smith[18] for a diatomic molecule. M. Baer generalized the formulation of diabatization for a given sub-Hilbert space (SHS) for reactions involving atom-molecule collisions by integrating the coupled differential equations along two-dimensional contour.[5,19,20] It was predicted

Received: September 25, 2019
Published: January 31, 2020

that the aforementioned transformation is only possible when the vector fields created by NACTs satisfy the "curl conditions".[20,21] This condition demands the existence of a sub-Hilbert space in the interested domain of nuclear CS and the nonremovable (transverse) components of NACTs are negligibly small. While integrating the NACTs along a closed contour encircling degenerate point(s) or passing through the points of a seam, resulting ADT angles attain the magnitude of integral multiple of π[22,23] bearing the signature of encapsulated conical intersection(s) (CI). Adhikari et al. generalized the beyond Born−Oppenheimer (BBO) treatment for three to six coupled electronic states and devised explicit expressions of NACTs, curl conditions, curl-divergence equations, ADT equations and diabatic PESs in terms of ADT angle(s).[24−29] For numerical calculations, those equations are also successfully implemented on various model[24−26,30] as well as realistic molecular systems.[27,28,31−34]

Though a first principle based BBO formalism is required for the construction of numerically accurate diabatic surfaces to calculate various dynamical observables of spectroscopic and scattering processes,[29] a generalized algorithm and software package is not available so far for diabatization of any "*N*" coupled electronic manifold with "*M*" nuclear degrees of freedom (DOFs). In this work, we take an initiative to develop a generalized algorithm "ADT" and a program to solve the ADT equations numerically associated with any number of nuclear DOFs for the given set of coupled electronic states. Due to the stiffness of the differential equations with singularly high magnitude of NACT at degenerate point, 8th order Runge−Kutta method is used to integrate those coupled differential (linear) equations. Moreover, in order to validate the utility of this developed algorithm and program package for realistic molecular species, we deliberately choose six such systems involved with variety of complexity in nonadiabaticity, namely, NO_2 radical,[34,35] H_3^+,[33,36] F + H_2,[37,38] NO_3 radical,[27,39,40] $C_6H_6^+$,[27] and 1,3,5-$C_6H_3F_3^+$ (TFBZ$^+$)[28] radical cation representing two, three, five, and six state sub-Hilbert spaces.

Nitrogen dioxide (NO_2) molecule exhibits profound nonadiabatic interactions within its lowest two electronic states (X^2A_1 and A^2B_2), which can resolve complicacies in assigning the theoretical photoelectron spectrum[34,35,41−46] with the experimental[47] one. Similarly, NO_3^- manifests highly complex spectral envelop[40,48] due to Jahn−Teller (JT) and pseudo Jahn−Teller (PJT) couplings within the low-lying five electronic states, $\tilde{X}^2A_2'$ (1^2B_2), $\tilde{A}^2E''$ (1^2A_2 and 1^2B_1) and $\tilde{B}^2E'$ (1^2A_1 and 2^2B_2) of the neutral analogue around the Franck−Condon (FC) region of nuclear CS.[27,39,40,48,49] The photoelectron spectra of C_6H_6 (Bz)[50] and 1,3,5-$C_6H_3F_3$ (TFBZ)[51] also exhibit highly structured spectral band originated from the lowest five ($\tilde{X}^2E_{1g}$, $\tilde{B}^2E_{2g}$ and $\tilde{C}^2A_{2u}$)[27,52,53] and six ($\tilde{X}^2E''$, $\tilde{A}^2A_2''$, $\tilde{B}^2E'$ and $\tilde{C}^2A_2'$)[28,54] coupled electronic states of Bz^+ and TFBZ$^+$, respectively. Our group has constructed highly accurate diabatic PESs of NO_2,[34,35] NO_3,[27,39] $C_6H_6^+$,[27] and 1,3,5-$C_6H_3F_3^+$,[28] employing ADT algorithm over pairwise normal modes, and simulated the photoelectron spectra of NO_2^-[34,47] and NO_3^-[40,48] anions already. In the realm of reaction dynamics, singlet H_3^+ appears as a center of attraction in the community mainly due to the experimental evidence as molecular species.[55] The global diabatic surfaces of H_3^+ computed by ADT algorithm considering three lowest electronic states ($1^1A'$, $2^1A'$ and $3^1A'$)[33] have been used to monitor the course of the reaction (D^+ + H_2) to calculate the integral cross sections (ICS)[36] of various quantum processes. On the other hand, F+H_2 is one of the demanding reactive system due to strong correlation among the electrons, profound spin−orbit effects due to open-shell F atom and intense nonadiabatic interactions.[37,38,56−58] Adhikari et al.[37,38] have calculated global diabatic PESs of three low-lying electronic states ($1^2A'$, $1^2A''$ and $2^2A'$) of F + H_2 with the advent of the present algorithm, which will be employed to carry out dynamical calculations in near future.

The article is organized as follows: section 2 depicts the theoretical formulation of BBO equations for "*N*" coupled electronic states of a molecular process. On the other hand, section 3 describes the theoretical validity on the workability of *N* electronic state "ADT" program for *M* nuclear DOFs and section 4 depicts a comprehensive discussion between BBO theory based ADT algorithm and other contemporary approaches for diabatization. Section 5 presents a brief description of the algorithmic framework while in section 6, the outcome of test runs is thoroughly analyzed. Finally, the summary of the present work is laid out in section 7. In order to provide a better overview of this algorithm and program, an extensive demonstration of the components of "ADT-version0" directory and the key instructions of "ADT" program package are documented in the Supporting Information (see sections S4 and S5) and user_manual.pdf.

2. BEYOND BORN−OPPENHEIMER THEORY

According to the BO treatment, total molecular wave function can be depicted as a linear combination of eigenfunctions of electronic Hamiltonian and the combining coefficients appear as the nuclear wave function.[1,2] Total electron−nuclear wave function for a *N*-dimensional sub-Hilbert space can be manifested as,

$$|\Psi(s_e, s_n)\rangle = \sum_{i=1}^{N} \psi_i^{\mathrm{ad}}(s_n)|\xi_i(s_e|s_n)\rangle \tag{1}$$

where the existence of *N* electronic state subspace requires theoretical as well as numerical justification for each molecular species/processes. The aforementioned wave function satisfies the following time-independent SE and the respective eigenvalue resembles the total energy of the system:

$$\hat{\mathbf{H}}(s_e, s_n)|\Psi(s_e, s_n)\rangle = E|\Psi(s_e, s_n)\rangle \tag{2}$$

Moreover, the molecular Hamiltonian $[\hat{\mathbf{H}}(s_e, s_n)]$ can be segregated into nuclear kinetic energy operator ($\hat{\mathbf{T}}_n$) and the electronic Hamiltonian $[\hat{\mathbf{H}}_e(s_e|s_n)]$,

$$\hat{\mathbf{H}}(s_e, s_n) = \hat{\mathbf{T}}_n(s_n) + \hat{\mathbf{H}}_e(s_e|s_n) \tag{3}$$

where the nuclear kinetic energy operator takes the following form:

$$\hat{\mathbf{T}}_n = -\frac{1}{2}\sum_i \left(\frac{\nabla^2_{s_n,i}}{m_i}\right) \tag{4}$$

On the other hand, the electronic wave functions $[|\xi_i(s_e|s_n)\rangle]$, the basis set for the BO expansion are considered as eigenfunctions of $\hat{\mathbf{H}}_e(s_e|s_n)$ with nuclear coordinate dependent eigenvalue, $u_i(s_n)$, where the electronic eigenvalue equation can be expressed as,

$$\hat{\mathbf{H}}_e(s_e|s_n)|\xi_i(s_e|s_n)\rangle = u_i(s_n)|\xi_i(s_e|s_n)\rangle \tag{5}$$

When the BO expansion of molecular wave function [eq 1] and the total Hamiltonian [eq 3] are plugged into the SE [eq 2],

https://dx.doi.org/10.1021/acs.jctc.9b00948
J. Chem. Theory Comput. 2020, 16, 1666−1680

and those equations are projected with various electronic eigenfunctions, the compact matrix equation of adiabatic (kinetically coupled) SE can be written as

$$\left[-\frac{1}{2}(\vec{\nabla}_n + \vec{\tau})^2 + \mathbf{U} - \mathbf{E}\right]\boldsymbol{\psi}^{\mathbf{ad}} = \mathbf{0} \tag{6}$$

where $\mathbf{U}_{ij} = u_i\delta_{ij}$ is the adiabatic potential energy matrix and $\vec{\boldsymbol{\tau}}$ is the nonadiabatic coupling matrix (NACM) defined as

$$\vec{\tau}_{ij} = \langle \xi_i(s_e|s_n)|\vec{\nabla}_n \xi_j(s_e|s_n)\rangle = \frac{\langle \xi_i(s_e|s_n)|\vec{\nabla}_n \hat{\mathbf{H}}_e(s_e|s_n)\xi_j(s_e|s_n)\rangle}{u_j - u_i} \tag{7}$$

For real electronic wave functions, eq 7 depicts the skew-symmetric form of $\vec{\boldsymbol{\tau}}$ matrix with the following form for N coupled electronic states:

$$\vec{\boldsymbol{\tau}} = \begin{pmatrix} 0 & \vec{\tau}_{12} & \vec{\tau}_{13} & \cdots & \vec{\tau}_{1,N-1} & \vec{\tau}_{1,N} \\ -\vec{\tau}_{12} & 0 & \vec{\tau}_{23} & \cdots & \vec{\tau}_{2,N-1} & \vec{\tau}_{2,N} \\ \vdots & \vdots & \ddots & & \vdots & \vdots \\ -\vec{\tau}_{1,N-1} & -\vec{\tau}_{2,N-1} & -\vec{\tau}_{3,N-1} & \cdots & 0 & \vec{\tau}_{N-1,N} \\ -\vec{\tau}_{1,N} & -\vec{\tau}_{2,N} & -\vec{\tau}_{3,N} & \cdots & -\vec{\tau}_{N-1,N} & 0 \end{pmatrix} \tag{8}$$

Moreover, eq 7 predicts that the NACTs blow up at the close vicinity of degenerate points, and thereby, the solution of adiabatic SE becomes numerically inaccurate. Considering this issue of adiabatic representation, it is inevitable to develop a different representation (diabatic) such that the singular kinetic couplings can be transformed into continuous, smooth and single-valued potential coupling terms. Such transformation can be readily achieved by using an orthogonal rotation matrix, which is labeled as $\mathbf{A}$. In this orthogonal transformation, $\boldsymbol{\psi}^{\mathbf{ad}}$ and $\boldsymbol{\phi}^{d}$ signify adiabatic and diabatic nuclear wave functions:

$$\boldsymbol{\psi}^{\mathbf{ad}} = \mathbf{A}\boldsymbol{\phi}^{\mathbf{d}} \tag{9}$$

While incorporating the above-mentioned "transformed" nuclear wave function in eq 6, diabatic representation of the nuclear SE can be formulated as

$$-\frac{1}{2}\nabla_n^2\boldsymbol{\phi}^{\mathbf{d}} + (\mathbf{W} - \mathbf{E})\boldsymbol{\phi}^{\mathbf{d}} = \mathbf{0} \tag{10}$$

where

$$\mathbf{W} = \mathbf{A}^{\dagger}\mathbf{U}\mathbf{A} \tag{11}$$

under the condition

$$\vec{\nabla}_n\mathbf{A} + \vec{\boldsymbol{\tau}}\mathbf{A} = \mathbf{0} \tag{12}$$

known as adiabatic-to-diabatic transformation (ADT) condition.[19]

For a N dimensional electronic manifold, the model form of ADT matrix $\mathbf{A}$ can be considered as a product of Λ $(={}^{N}C_2 = \frac{N(N-1)}{2})$ elementary rotation matrices constituted with mixing angles between any two electronic states for the N-state SHS. The elements of any of this rotation matrix, $\mathbf{A}^{mn}(\Theta_{mn})$ are defined as

$$[\mathbf{A}^{mn}(\Theta_{mn})]_{mm} = \cos\Theta_{mn} = [\mathbf{A}^{mn}(\Theta_{mn})]_{nn};\ m \neq n$$

$$[\mathbf{A}^{mn}(\Theta_{mn})]_{mn} = \sin\Theta_{mn} = -[\mathbf{A}^{mn}(\Theta_{mn})]_{nm};\ m \neq n$$

$$\text{and } [\mathbf{A}^{mn}(\Theta_{mn})]_{ij} = \delta_{ij};\ \{i, j\} \neq \{m, n\}.$$

The product of those rotation matrices can be arranged in $\Lambda!$ possible ways and thereby, the model form of $\mathbf{A}$ matrix can be written as:

$$\mathbf{A} = P_n\{\mathbf{A}^{12}(\Theta_{12})\cdot\mathbf{A}^{13}(\Theta_{13})\cdot\mathbf{A}^{23}(\Theta_{23})\ldots\mathbf{A}^{N-1,N}(\Theta_{N-1,N})\},$$
$$n = 1, \ldots, \Lambda! \tag{13}$$

where P_n is the nth permutation between two rotational matrices and $\{\Theta_{ij}\}$s are the nuclear coordinate dependent ADT angles. A representative example of one of such matrix for a five-state SHS can be given as:

$$\mathbf{A}^{14}(\Theta_{14}) = \begin{pmatrix} \cos\Theta_{14} & 0 & 0 & \sin\Theta_{14} & 0 \\ 0 & 1 & 0 & 0 & 0 \\ 0 & 0 & 1 & 0 & 0 \\ -\sin\Theta_{14} & 0 & 0 & \cos\Theta_{14} & 0 \\ 0 & 0 & 0 & 0 & 1 \end{pmatrix}$$

The ADT condition (eq 12) can be employed as the predecessor of formulating the ADT equations. One can carry out the formulation of ADT equation by choosing a particular order of multiplication in eq 13, since the numerical solution of those equations for any arrangement will be same (see section 3.1 and subsection S1.2 of the Supporting Information).

When the *ab initio* calculated components of $\vec{\boldsymbol{\tau}}$ matrix elements (eq 8) and model form of $\mathbf{A}$ matrix (eq 13) are stuffed into eq 12, one obtains a relation between the set of the gradients of the ADT angles with the NACTs, according to the following matrix equation:

$$\begin{pmatrix} G_{11} & G_{12} & G_{13} & \cdots & G_{1N} \\ G_{21} & G_{22} & & & \\ G_{31} & & \ddots & & \vdots \\ \vdots & & & & \\ G_{N1} & & \cdots & & G_{NN} \end{pmatrix}\cdot\begin{pmatrix} \vec{\nabla}\Theta_{12} \\ \vec{\nabla}\Theta_{13} \\ \vec{\nabla}\Theta_{23} \\ \vdots \\ \vec{\nabla}\Theta_{N-1,N} \end{pmatrix} = \begin{pmatrix} T_{11} & T_{12} & T_{13} & \cdots & T_{1N} \\ T_{21} & T_{22} & & & \\ T_{31} & & \ddots & & \vdots \\ \vdots & & & & \\ T_{N1} & & \cdots & & T_{NN} \end{pmatrix}\cdot\begin{pmatrix} \vec{\tau}_{12} \\ \vec{\tau}_{13} \\ \vec{\tau}_{23} \\ \vdots \\ \vec{\tau}_{N-1,N} \end{pmatrix} \tag{14}$$

where $\{G_{ij}\}$s and $\{T_{ij}\}$s are trigonometric functions of the ADT angles $\{\Theta_{ij}\}$s. Simplification of the above relation will lead to a set of Λ unique coupled differential equations of the form

$$\vec{\nabla}_n\Theta_{ij} = \sum_{m=1}^{\Lambda} c^{(m)}\vec{\tau}_{(m)} \tag{15}$$

where $\{c^{(m)}\}$s are scalar functions of ADT angles $\{\Theta_{kl}\}$. As for example, the explicit forms of ADT equations for four and five

https://dx.doi.org/10.1021/acs.jctc.9b00948
J. Chem. Theory Comput. 2020, 16, 1666−1680

coupled electronic states are presented in the Supporting Information (see sections S2 and S3).

At each and every grid point in the interested domain of nuclear CS, *ab initio* calculated NACTs ($\vec{\tau}_{kl}$) for each component are plugged into eq 15 and those equations are numerically integrated to obtain the ADT angles. Once the ADT angles are in hand, a similarity transformation (eq 11) is performed for transmuting the singular nature of NACTs in the form of smooth/continuous diagonal and off-diagonal diabatic (potential) coupling elements.

It is worthwhile to mention that if nonadiabatic interactions are overlooked, inconsistency between the theoretically predicted and experimentally probed spectra/cross sections is maximum over the energy domain, in particular where Jahn−Teller (JT)/Renner−Teller (RT) as well as accidental CIs are located. Only diabatized PESs based on BBO theory can predict highly accurate transition probabilities or sufficiently precise integral cross sections.[29]

3. "ADT" ALGORITHM FOR *N* ELECTRONIC STATES AND *M* NUCLEAR DOFS

The present version of BBO theory and its numerical implementation is completely general for N dimensional sub-Hilbert space of electronic states involving M nuclear DOFs, where the quantum chemistry packages can provide the nonadiabatic coupling matrix elements ($\tau_{ij}^{Q_k}(\{Q_k\})$, $k \in M$) between any two electronic states ($i, j \in N$) and adiabatic PESs for each electronic state as functions of "M" DOFs. On plugging those coupling elements ($\tau_{ij}^{Q_k}(\{Q_k\})$) in ADT equation (eq 15), we need to solve the ADT angles along a contour or over a set of contours, namely, line integrals over enclosed paths for two or more than two nuclear DOFs, respectively. The advantage of such an approach is to get the benefit of Cauchy's residue theorem leading to the value of ADT angle with $n\pi$ if the path of contour integral encloses singularity(ies) in the functional form of NACT. Therefore, if the nuclear CS consists three (3) DOFs, one can perform such integration on a set of 2D cross sections of the original 3D space (see Figure 1) and such approach can be extended for systems with "M" DOFs.

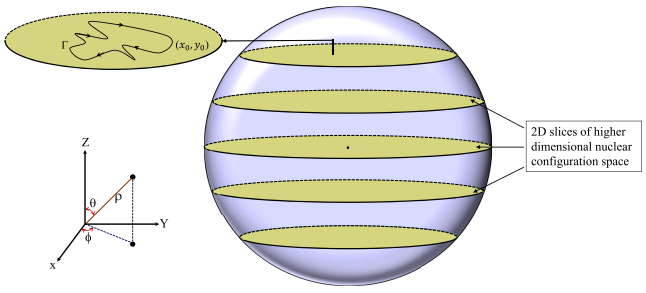

Figure 1. Diagram represents the contour of ADT over a 2D slice extracted from three-dimensional nuclear CS.

Considering well-known JT and RT physics for spectroscopic processes dominated around FC region leading to photoelectron or photoabsorption spectra, the nonadiabatic effects have been modeled through "linear" and "bilinear" diabatic couplings for each pair of normal modes. As for example, the JT/RT diabatic Hamiltonian constructed with quasi-diabatic approach[59,60] for spectroscopic processes of floppy molecules depicting nonadiabatic effect from N electronic states is given by,

$$\mathbf{H} = H_0\mathbf{I} + \mathbf{W} \tag{16}$$

where,

$$H_0 = \frac{1}{2}\sum_{k=1}^{M}\omega_k\left(-\frac{\partial^2}{\partial Q_k^{\,2}} + Q_k^{\,2}\right) \tag{17}$$

$$W_{ij} = \sum_{k=1}^{M}\lambda_k Q_k + \sum_{k,l(k\neq l)}^{M}\gamma_{kl}Q_kQ_l \tag{18}$$

and $\mathbf{I}$ designates an unit matrix of order $N \times N$ for N electronic states. In the above expressions, $\{\omega_k\}$ represent fundamental frequencies of normal modes and $\{\lambda_k\}$, $\{\gamma_{kl}\}$ denote the combining coefficients of linear and bilinear terms, respectively. Thus, in case of spectroscopic processes, since the electron−nuclear coupling is approximately accounted by considering pairwise nuclear DOFs, the solution of ADT equations *vis-à-vis* contour integrations have been carried out only over two nuclear DOFs at a time. On the contrary, ADT can provide numerically "exact" coupling terms between any pair of such modes, where the fitted functional form could contain all order of polynomials.[27,28,31,34,40] In other words, the general form of the coupling term originating from ADT for a pair of modes would be

$$W_{ij} = \sum_{k=1}^{M}\sum_{p}\lambda_{k,p}Q_k^{\,p} + \sum_{k,l(k\neq l)}^{M}\sum_{p,q}\gamma_{kl,\mathrm{pq}}Q_k^{\,p}Q_l^{\,q} \tag{19}$$

On the other hand, those effects in scattering problem (triatomic reaction) strongly diffuse from the interaction region to the asymptote and thereby, the associated ADT equations need to be solved over the set of 2D contours of the 3D nuclear CS. Thus, the diabatic Hamiltonian for a triatomic scattering system is presented as,[36]

$$\mathbf{H} = \left\{-\frac{\hbar^2}{2\mu_R}\frac{\partial^2}{\partial\rho^2} + \frac{2}{\mu_R\rho^2}\mathrm{L}^2(\theta,\phi) + \frac{J^2 - J_z^{\,2}}{\mu_R\rho^2\cos^2\theta} + \frac{J_z^{\,2} - 4\cos\theta\, J_zP_\phi}{2\mu_R\rho^2\sin^2\theta} + \frac{\sin\theta}{\mu_R\rho^2\cos^2\theta}\frac{1}{2}[J_+^{\,2} + J_-^{\,2}]\right\}\mathbf{I} + \mathbf{V}(\rho,\theta,\phi) \tag{20}$$

where ρ, θ, and ϕ are the hyperspherical coordinates. For three electronic states, $\mathbf{I}$ signifies a 3×3 unit matrix, $\mathbf{V}$ symbolizes the interaction diabatic potential matrix (3×3) among those states, and the rest of the operators are specified elsewhere.[61] It is important to note that the off-diagonal elements of $\mathbf{V}$ (originated from nonadiabatic interactions) appear as the functions of ρ, θ, and ϕ in the total Hamiltonian. While constructing the diabatic Hamiltonian for such triatomic scattering system, the solution of the ADT equation (eq 15) has been carried out over $\theta - \phi$ space at each fixed ρ value to calculate the ADT angles, $\Theta_{ij}(\rho, \theta, \phi)$s and then, to transform the adiabatic SE to a diabatic one.[33,36]

3.1. Illustration of ADT Algorithm on H + H_2 Collision Process.

We consider the collision process on H+H_2 system to illustrate the scheme in the ADT algorithm as presented in section 2. The theoretical treatment has been carried out considering 3-state ($N = 3$) SHS.

We define the nuclear CS by selecting Jacobi coordinates $\vec{r}$, $\vec{R}$, and γ, which are the H−H diatomic distance (r), the distance of third H atom from the midpoint of the H−H diatom (R), and the angle between $\vec{r}$ and $\vec{R}$ (γ) as represented in Figure 2. In this

https://dx.doi.org/10.1021/acs.jctc.9b00948
J. Chem. Theory Comput. 2020, 16, 1666−1680

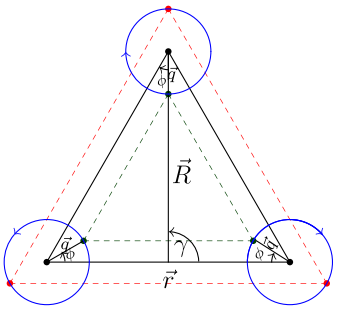

Figure 2. Nuclear configuration space of the H + H_2 system is defined by the Jacobi coordinates: $\vec{r}$, $\vec{R}$, and γ. To define the contour, three loops of the corresponding H atoms are formed with equal radii (q = 0.1 Å) encircling the center points (black dots) defined by r = 1.0 Å, R = 0.866 Å, and γ = 90° (D_{3h} point). ϕ is the angle of rotation of H atoms along those loops, where the directions of rotation are also indicated by blue arrows. In this contour, for two specific ϕ values, the system attains D_{3h} configuration represented by the outer and inner dashed triangles with red and green colors, respectively.

nuclear manifold, the lowest three adiabatic states ($1^2A'$, $2^2A'$ and $3^2A'$) of H + H_2 are nonadiabatically coupled. There occurs a JT symmetry required D_{3h} CI seam between $1^2A'$ and $2^2A'$ states, which are also vibronically coupled to the second excited state ($3^2A'$). The nuclear geometries are expressed in terms of polar coordinates q and ϕ corresponding to the radii and angle of traversing around loops formed by H atoms, respectively, with center points at the original positions of those atoms (see Figure 2).

The ADT matrix for the 3-state SHS will be given by

$$\mathbf{A}(\Theta_{12}, \Theta_{23}, \Theta_{13}) = \mathbf{A}^{12}(\Theta_{12})\cdot\mathbf{A}^{23}(\Theta_{23})\cdot\mathbf{A}^{13}(\Theta_{13}) \quad (21)$$

whereas the diabatic matrix is

$$\mathbf{W} = \mathbf{A}^{\dagger}(\Theta_{12}, \Theta_{23}, \Theta_{13})\mathbf{U}\mathbf{A}(\Theta_{12}, \Theta_{23}, \Theta_{13}) \quad (22)$$

where Θ_{ij} are the ADT angles and are functions of the nuclear coordinates q and ϕ. The explicit form of the ADT and the diabatic matrix elements (eqs 21 and 22) are presented in the Supporting Information (see subsection S1.1). With the following form of the NACM:

$$\vec{\tau}(q, \phi) = \begin{pmatrix} 0 & \vec{\tau}_{12}(q, \phi) & \vec{\tau}_{13}(q, \phi) \\ -\vec{\tau}_{12}(q, \phi) & 0 & \vec{\tau}_{23}(q, \phi) \\ -\vec{\tau}_{13}(q, \phi) & -\vec{\tau}_{23}(q, \phi) & 0 \end{pmatrix}$$

the two sets of scalar components of the ADT equations (eq 15) will be

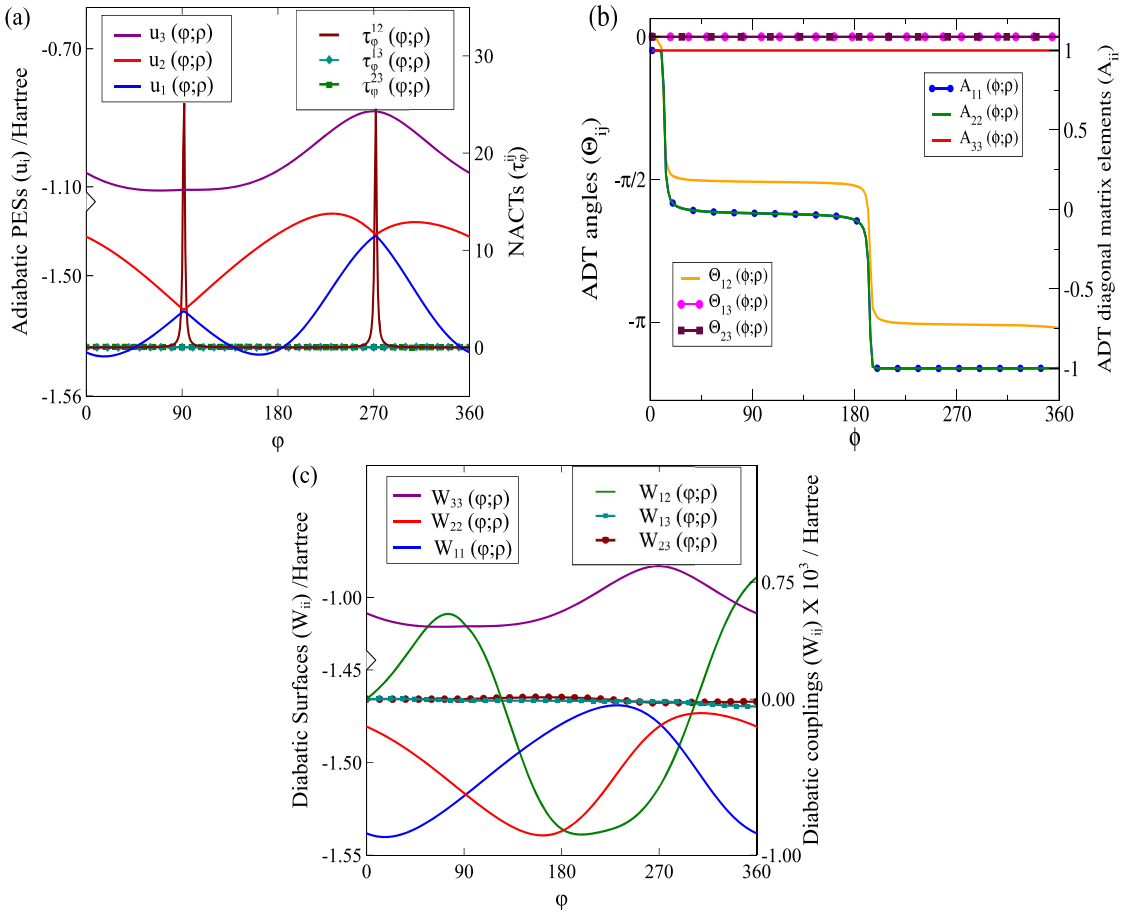

Figure 3. (a) Lowest three adiabatic PESs and the NACTs between the states ($1^2A'$, $2^2A'$ and $3^2A'$) of H+H_2 system along ϕ coordinate for a fixed q value (= 0.1 Å). (b) Solution of the ADT equations Θ_{ij} and the diagonal ADT matrix elements ($\mathbf{A}_{ij}$). Θ_{12} reaches the magnitude π at the closed contour ($\phi = 2\pi$), and $\mathbf{A}_{11}$ and $\mathbf{A}_{22}$ change sign validating the presence of one JT CI seam along the chosen contour. The other angles Θ_{13} and Θ_{23} are close to zero, and $\mathbf{A}_{33}$ remains almost unity. (c) Diabatic potential energy matrix elements, which appear to be smooth, single-valued and continuous functions of nuclear coordinates.

https://dx.doi.org/10.1021/acs.jctc.9b00948
J. Chem. Theory Comput. 2020, 16, 1666−1680

$$\frac{\partial \Theta_{12}}{\partial q} = -\tau_q^{12} + \tan \Theta_{23}(\tau_q^{13} \cos \Theta_{12} - \tau_q^{23} \sin \Theta_{12}),$$

$$\frac{\partial \Theta_{12}}{\partial \phi} = -\tau_\phi^{12} + \tan \Theta_{23}(\tau_\phi^{13} \cos \Theta_{12} - \tau_\phi^{23} \sin \Theta_{12}),$$

$$\frac{\partial \Theta_{13}}{\partial q} = -(\tau_q^{13} \sin \Theta_{12} + \tau_q^{23} \cos \Theta_{12}),$$

$$\frac{\partial \Theta_{13}}{\partial \phi} = -(\tau_\phi^{13} \sin \Theta_{12} + \tau_\phi^{23} \cos \Theta_{12}),$$

$$\frac{\partial \Theta_{23}}{\partial q} = -\frac{1}{\cos \Theta_{23}}(\tau_q^{13} \cos \Theta_{12} - \tau_q^{23} \sin \Theta_{12}),$$

$$\frac{\partial \Theta_{23}}{\partial \phi} = -\frac{1}{\cos \Theta_{23}}(\tau_\phi^{13} \cos \Theta_{12} - \tau_\phi^{23} \sin \Theta_{12}). \quad (23)$$

The NACTs (τ_q^{ij} and τ_ϕ^{ij}) are obtained by MOLPRO quantum chemistry package[62] using complete active space self-consistent field (CASSCF) level of methodology. The differential equations (eq 23) are solved over 2D contour as functions of q and ϕ by employing backward differential formula with appropriate relative and absolute error tolerance to achieve the convergence. When we solve eq 23, all the ADT angles (Θ_{ij}) are arbitrarily chosen as zero (0) at $\phi = 0$ and $q = 0.1$ Å.

Figure 3a displays the adiabatic PESs u_i and the NACT components τ_ϕ^{ij} in a 1D cut along ϕ coordinate at $q = 0.1$ Å. The JT CI seam between the lowest two states intersects the contour at two different positions of ϕ coordinate, where the magnitude of τ_ϕ^{12} shows singular nature. Since the third state (u_3) is adiabatically separated from the lowest two states, the two NACT components τ_ϕ^{13} and τ_ϕ^{23} are very close to zero. The solution of eq 23 gives functional forms of $\Theta_{ij}(q, \phi)$ where Θ_{12} reaches π at $\phi = 2\pi$ for $q = 0.1$ Å. Also, there is single sign change of $\mathbf{A}_{11}$ and $\mathbf{A}_{22}$ elements which validate the existence of one JT CI seam in the given nuclear CS, as shown in Figure 3b. Figure 3c exhibits those diabatic potential energy diagonal as well as off-diagonal (coupling) matrix elements along the same ϕ coordinate. It is evident that such elements are now smoothly varying functions of nuclear coordinates, and $\mathbf{W}_{11}$ and $\mathbf{W}_{22}$ cross each other at those intersection points.

ADT can also be performed with $\mathbf{A}$ matrix constructed with a different order of multiplication of elementary rotation matrices as shown in eq 13. Although the explicit expressions of ADT matrix elements, ADT equations and diabatic matrix elements appear different with the choice on the order of multiplication of elementary rotation matrices, the solutions of eq 15 remain same. In other words, the magnitude of the ADT angles are same up to a sign and thereby, the diabatic potential matrix elements are invariant. This has been illustrated in Supporting Information (see subsection S1.2), where those quantities are derived for the $H + H_2$ system with a different order of $\mathbf{A}$ matrix.

4. ADT ALGORITHM *VIS-À-VIS* OTHER APPROACHES

The ADT algorithm and program is based on BBO approach which is theoretically and numerically "exact" enabling us to compute accurate diabatic potential energy matrix from *ab initio* calculated adiabatic PESs and NACTs. Our studies involve both spectroscopic and scattering processes where nonadiabatic description is required—not necessarily only around the FC region but also up to the asymptotes.[29] In this section, we discuss the BBO theory based ADT algorithm in comparison with other contemporary methodologies which can include the contributing electronic states on a process, namely ground and relevant excited states.

- In BBO theory, the molecular wave function is expanded in terms of the product form of the electronic (adiabatic) eigenfunctions (see eq 1): $|\Psi(s_e, s_n)\rangle = \sum_{i=1}^{N} \psi_i^{ad}(s_n)|\xi_i(s_e|s_n)\rangle$, which can be rewritten in an alternative (diabatic) representation as $\Psi(s_e, s_n) = \sum_i \psi_i^{ad}(s_n)\ \mathbf{A}(s_n)\tilde{\xi}_i(s_e) = \sum_i \psi_i^{dia}(s_n)\tilde{\xi}_i(s_e)$. Such a transformation by $\mathbf{A}(s_n)$ matrix removes the nuclear coordinate dependence of $\xi_i(s_e|s_n)$ to an arbitrary function $\tilde{\xi}_i(s_e)$. As a result, the NACTs vanish from adiabatic SE, leading to diabatic potential couplings. It is possible to find a theoretically and numerically "exact" form of $\mathbf{A}(s_n)$ matrix by solving eq 15 and $\mathbf{W}(s_n)$ by substituting $\mathbf{A}(s_n)$ in eq 11 at each point (s_n) in the nuclear CS. As a result, the BBO theory based diabatization can generate global PESs, particularly for scattering processes, where the nonadiabatic interactions appear frequently at asymptotes. Even for spectroscopic processes, the accidental degeneracies away from the given reference point or seam can be accurately described by the BBO approach. On the contrary, the vibronic coupling model (VCM)[59] was developed based on an *ansatz*, where the diabatic diagonal as well as off-diagonal (coupling) matrix elements are assumed to be linear and bilinear functions of nuclear coordinates with respect to the minima of the ground adiabatic PES ($V_0(s_n)$) or a CI point ($s_{n,0}$) for better applicability.[63−65] In other words, for linear VCM, it is developed based on the Taylor series expansion of diabatic matrix elements around a reference nuclear configuration $s_{n,0}$ as

$$W_{ii}(s_n) = \hat{T}_{nuc} + V_0(s_n) + W_{ii}(s_{n,0}) + \sum_q \kappa_q^{(i)} s_q$$

$$W_{ij}(s_n) = \sum_q \lambda_q^{(i,j)} s_q;\ \ i \neq j, \quad (24)$$

where W_{ij} are the diabatic potential energy matrix elements, $\kappa_q^{(i)}$ and $\lambda_q^{(i,j)}$ are linear vibronic coupling constants. Though the model is derived based on such a crude approximation, it is generally valid close to the FC region around the molecular geometry $s_{n,0}$, particularly when the ground state does not have degeneracy.
- In BBO theory, the quantization of ADT angle(s) reaching the magnitude $n\pi$ (n being an integer) at the end of a closed contour is an important criterion to validate the presence of CI(s)/seam(s) (symmetry allowed or accidental) in the nuclear CS. This in turn guarantees the accuracy and nature of the diabatic potential energy matrix elements. On the other hand, the vibronic coupling model has no such analogous way of excluding the CI(s) in nuclear CS and judging the accuracy of the diabatic PESs.
- If one of the asymmetric stretching modes of a molecule generate symmetric functional form of adiabatic PESs and NACTs, the calculated diabatic coupling elements should retain the symmetric nature, but quasi-diabatic approach may fail to recognize such situations. For such normal modes, diabatic matrix elements can not show up odd power polynomial dependence rather would be con-

https://dx.doi.org/10.1021/acs.jctc.9b00948
J. Chem. Theory Comput. 2020, 16, 1666−1680

stituted of only even power terms. In several cases, the BBO theory based coupling elements have shown such features, namely, the lone asymmetric stretching mode of NO_2,[34] one of the asymmetric stretching and bending modes in NO_3 (ν_{3x} and ν_{4x}),[40] $C_6H_6^+$ (e.g., ν_{16x})[66] and 1,3,5-$C_6H_3F_3^+$ (e.g., ν_{9x}, ν_{10y} and ν_{12y}).[28]

- Quantum or semiclassical nonadiabatic dynamics for relatively larger molecular systems can equally employ the strategies of BBO methodology. On-the-fly diabatization version of multiconfigurational time-dependent Hartree (MCTDH)[67,68] and direct-dynamics variational multiconfigurational Gaussian (DD-vMCG)[69−71] are also notable approaches to carry out nonadiabatic dynamics. The algorithm of those methodologies are based on computing the ADT matrix $\mathbf{A}(s_n)$ using line integrals of the NACTs between any two adiabatic states at the close vicinity of a CI point/seam at each step of propagation:[70]

$$\vec{\nabla}_n \mathbf{A}(s_n) = -\vec{\boldsymbol{\tau}}(s_n)\mathbf{A}(s_n) \tag{25}$$

for which the solution is known to be of the form[20,72]

$$\mathbf{A}(s_n + \Delta s_n) = \exp\left(-\int_{s_n}^{s_n+\Delta s_n} \vec{\boldsymbol{\tau}}\cdot \mathrm{d}\vec{s}_n\right)\mathbf{A}(s_n)$$

One can invoke BBO theory based ADT algorithm, as presented in this article, to provide a more formal solution of eq 25. In other words, eq 15 can provide more accurate results including all the required number of electronic states to constitute the SHS at regions of strong nonadiabaticity among those states.

5. PROGRAM STRUCTURE OF "ADT"

5.1. Framework of "ADT" Program. A detailed description on the components of package directory ("ADT-version0") are demonstrated in Figure 4 and in the Supporting Information (see section S4). The parent folder contains one python file "setup.py", which is dedicated to execute the installation of "ADT" software package. On the other hand, the subdirectory, "adt" contains necessary source files for analytic formulation, numerical computation and interfacing MOLPRO package prior to numerical calculation. The "analytic" segment inside "adt" directory is used to formulate symbolic expressions of six different ADT quantities, namely, ADT matrices, partial and complete substituted ADT equations (see section S4 of the Supporting Information for details), coefficient matrices (**G** and **T**, see eq 14) and diabatic potential energy matrices with the help of two python files, 'adt_analytic.py' and 'anamod.py'. On the other hand, 'adt_numeric.py' and 'nummod.f90' in "numeric" section are dedicated for accurate numerical integration of ADT equations (eq 15) along any one of the eight possible paths to compute ADT angles, ADT matrix elements, diabatic potential energy matrix elements and residue of ADT angles. The other segment, "molpro" contains one interfacing python code, 'adt_molpro.py', which can carry out MOLPRO jobs with user provided inputs (MOLPRO keywords, atom information, equilibrium geometry, frequency and Wilson matrix) followed by numerical calculations of ADT quantities.

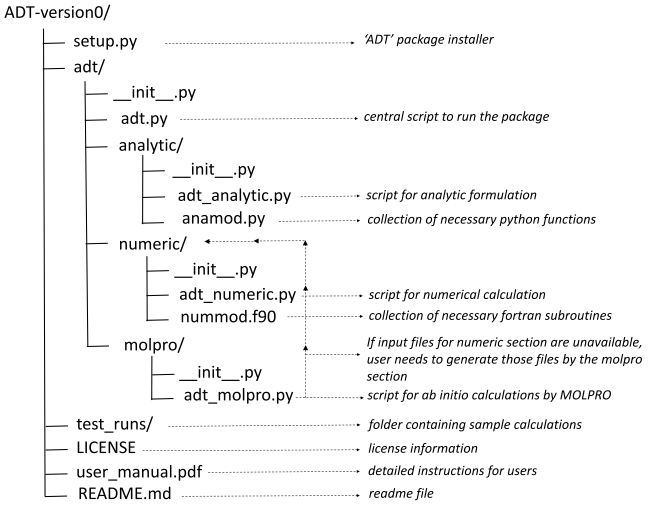

Figure 4. Directory structure depicting the files and directories present in the parent folder "ADT-version0".

5.2. Instructions and Work Flow of "ADT" Program. Functioning of "ADT" program entirely depends on the well-structured python and Fortran codes, which are developed for the first time in the realm of nonadiabatic dynamics. A brief sketch of the "ADT" program is presented in Figure 5. On the other hand, detailed instructions are vividly explained in the Supporting Information (see section S5) and also in "user_manual.pdf" with suitable examples. Once the program package is successfully installed, the command-line tool `adt` will be generated automatically, which can be used for execution by three subcommands, namely, `ana`, `num`, and `mol` to carry out analytic formulation, numerical computation, and interfacing of MOLPRO followed by numerical calculation, respectively.

- While generating analytic expressions for various ADT quantities, the user has to execute the `adt ana` command with three arguments (one mandatory and two optional) (see Figure 5).
- For numerical computation, one needs to specify 10 arguments (one mandatory and nine optional) for `adt num` command. Among those 10 arguments, the compulsory one indicates the locational path of the NACT file representing the component along the circular coordinate (see Figure 5), if the adiabatic PES and NACT files are available as input ones. In other words, there will be three input files (adiabatic PESs and two components of NACTs) for 2D calculation, whereas only two files (adiabatic PESs and angular component of NACTs) are necessary for executing 1D calculation along a closed circular path. Moreover, such calculation can also be performed by using "ADT" as a module in python script employing two in-built functions, "adt1d" and "adt2d".
- If the input files (adiabatic PESs and NACTs) need to be calculated by interfacing MOLPRO before numerical calculations are performed using "ADT", the `adt mol` command requires 11 arguments, two are compulsory and the rest are optional (see Figure 5). The user has to supply two input files (MOLPRO configuration file and atom information file) for both spectroscopic and scattering calculations, whereas the spectroscopic cases require three additional files (equilibrium geometry file, frequency file, and Wilson matrix file).

https://dx.doi.org/10.1021/acs.jctc.9b00948
J. Chem. Theory Comput. 2020, 16, 1666−1680

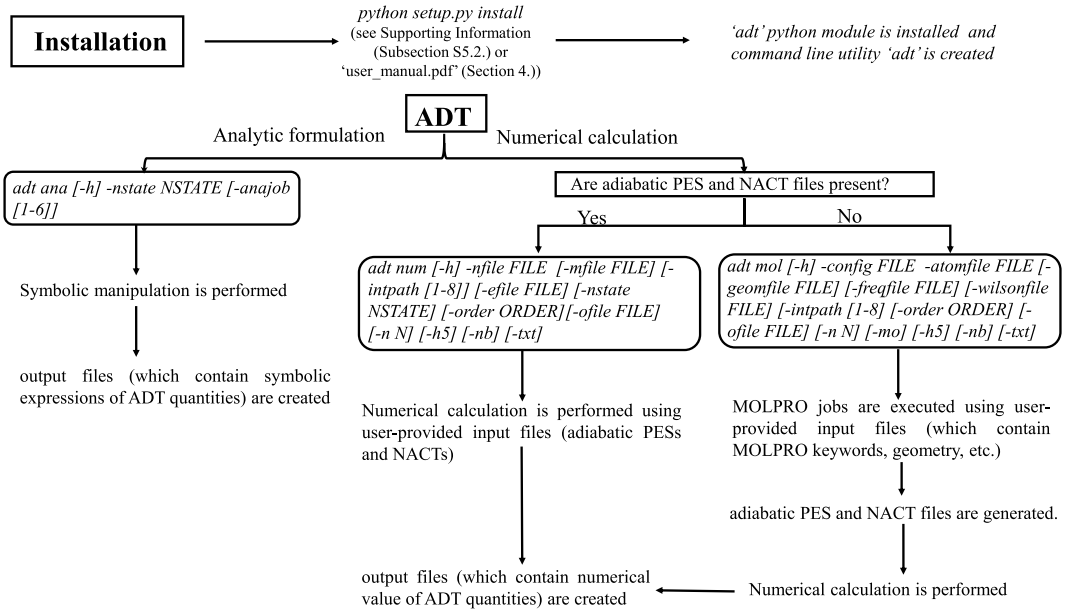

-h, --help	Help flag
-anajob [1-6]	Type of expression (default: 3 – completely substituted ADT equation)
-intpath [1-8]	Path for integration (default: 1).
-efile FILE	Energy file for calculating the diabatic potential energy matrix elements.
-nstate NSTATE (Analytic Section)	Number of states to do the analytical formulation.
-nstate NSTATE (Numeric Section)	Number of states to do the ADT calculation.
-ofile FILE	Path of Output file (default: 'ADT_numeric').
-order ORDER	Order of multiplication of elementary rotation matrices
-n N	Number of OpenMP threads for parallel jobs.
-h5/-nb/-txt	Output file in HDF5 (.h5) or numpy binary (.npy) or text (.dat) format, respectively (default is text format) .
-mo	Termination of execution after completion of only MOLPRO jobs
-mfile FILE	Path of NACT file representing the component along non-circular coordinate for 2D calculation
-nfile FILE	Path of NACT file representing the component along circular coordinate for 1D as well as 2D calculation
-config FILE	Path of MOLPRO config file.
-atomfile FILE	Path of the input file containing the information of atoms
-geomfile FILE	Path of the equilibrium geometry file (default: geomfile.dat) (necessary for spectroscopic systems).
-freqfile FILE	Path of the frequency file (default: freqfile.dat) (necessary for spectroscopic systems).
-wilsonfile FILE	Path of the Wilson matrix file (default: wilson.dat) (necessary for spectroscopic systems).

Figure 5. Overall schematic outline of the working principles for analytic expressions generation, numerical calculations, and molpro interfacing followed by ADT execution. Detailed description of the arguments `-anajob` and `-intpath` are presented in Tables 1 and 2 of the user_manual.pdf.

6. TEST RUNS

6.1. Study of Computational Efficiency. Efficiency and memory requirement of this code is thoroughly investigated in a workstation (processor: 20 M cache, 8 cores, 16 threads, 2.10 GHz and memory: 32 GB) for analytic expressions as well as numerical calculations. For analytic segment, we generate partially and fully substituted ADT equations for two to nine coupled electronic states, and the elapsed time is recorded in Table 1. It can be concluded that the increase in elapsed time is not linear with the number of electronic states. Initially, it grows very slowly, but the rate of increment increases with higher number of electronic states due to large and complicated structure of various ADT quantities, like, ADT equations. On the other hand, such a trend is more prominent for fully substituted ADT equations, and hence, the user can take the benefit of partially substituted ones for higher dimensional sub-Hilbert spaces to reduce the computation time.

For numerical calculations, this code is executed for two to ten electronic states with two DOFs varying at a time and others are kept at equilibrium geometries. Similarly, such calculations can be replicated considering two other nuclear DOFs while the rest of the modes are at equilibrium. Those calculations have been performed employing gFortran compiler in two different ways: (a) without any parallelization scheme and (b) with extensive OpenMP parallelization (using eight threads on eight processors). In addition, for each case, three different file

https://dx.doi.org/10.1021/acs.jctc.9b00948
J. Chem. Theory Comput. 2020, 16, 1666−1680

Table 1. Elapsed Time for Devising Partially and Fully Substituted ADT Equations (`-anajob 2` and `-anajob 3`)

	elapsed time (s)	
N	`-anajob 2`	`-anajob 3`
2	0.00094	0.00084
3	0.00100	0.00095
4	0.00161	0.00168
5	0.00331	0.00564
6	0.00806	0.01587
7	0.01230	0.12705
8	0.08721	2.05638
9	0.53056	34.59282

formatting systems are used (HDF5 or NumPy binary or text) in order to reveal their relative efficiency and fastness. Elapsed time is calculated precisely for two to ten coupled electronic states using 62500 grid points and presented in Figure 6. It is

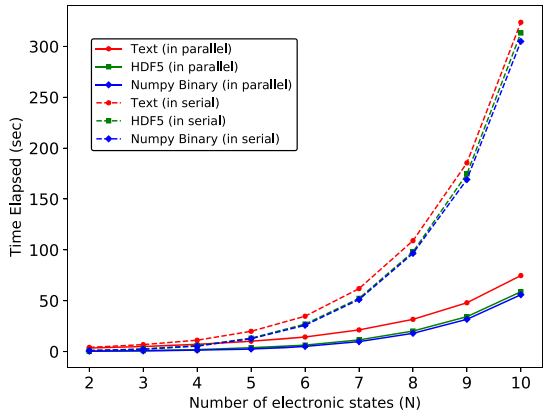

Figure 6. Variation of elapsed time with the increase in number of electronic states for two situations: (a) gFortran compiler without any parallelization and (b) gFortran compiler with OpenMP parallelization. The second scheme along with NumPy binary formatted input/output system is the most advantageous one.

worthwhile to mention that the parallel jobs (Figure 6) are more efficient ones and usage of NumPy binary formatted input/output files is the most advantageous due to fastness and easy portability. Though recorded runtime increases gradually with number of coupled electronic states, memory requirement is relatively very small and remains almost invariant. The figure clearly depicts the efficiency and workability of our software framework for diabatization of adiabatic SE for arbitrary "*N*" number of electronic states.

6.2. Analytical Test Runs. We perform formulation of some analytic expressions and those are placed in 'test_runs' folder (see Figure S3 of the Supporting Information). In order to provide a better understanding of the users, we formulate analytic expressions of four-state ADT equations and elements of diabatic potential energy matrix for five state sub-Hilbert space. Moreover, coefficient matrix of gradient of ADT angles for six coupled electronic states and coefficient matrix of NACTs for eight electronic manifold are also devised (see eq 14).

6.3. Numerical Test Runs. We numerically calculate ADT angles, ADT matrices, diabatic PESs matrices and residue of ADT angles for six realistic molecular systems/processes. The relevant data of input/output files is given in the 'test_runs' folder of "ADT-version0" directory (see Figure S3 of the Supporting Information). Once adiabatic PESs and NACTs are available as input files, one can run the numeric section only (see the details of the commands in the 'ADT-version0/test_runs/numerical_calculations/X/README.md' file, where X = NO2 or H3+_1D or H3+_2D or F+H2 or NO3 or C6H6+ or C6H3F3+) otherwise, if adiabatic PESs and NACTs need to be evaluated using MOLPRO followed by ADT calculation, the user can see the details of the commands in the 'README.md' file in the directory, 'ADT-version0/test_runs/molpro_numerical_calculations/X/' (X = NO2 or H3+_1D or H3+_2D or F+H2 or NO3 or C6H6+ or C6H3F3+). A brief summary for constructing the 'molpro.config' files for the spectroscopic (NO_2, NO_3, $C_6H_6^+$ and 1,3,5-$C_6H_3F_3^+$) and scattering (H_3^+ and $F+H_2$) systems is described in Tables 7 and 8 of user_manual.pdf, respectively.

6.3.1. NO_2 Radical. With two-state BBO theory, inherent nonadiabatic interactions prevalent in this notoriously difficult species have been studied and at the same time, nuclear dynamics has been performed to predict a theoretical photoelectron spectra.[34,35] Those investigations are revisited here to demonstrate the workability of the newly developed software framework for a set of two coupled electronic states. For NO_2 radical, we employ two normal modes, namely, bending and asymmetric stretching vibration (Q_1 and Q_3) to perform the *ab initio* calculations of adiabatic PESs as well as the NACT within those low-lying electronic states (X^2A_1 and A^2B_2 at C_{2v} geometry and a pair of $^2A'$ states at C_s geometry). CASSCF level of methodology is opted for calculating adiabatic PESs using Dunning's correlation consistent polarized valence triple-ζ (cc-pVTZ) basis set and 17 electrons in 11 orbitals (17e, 11o) configuration active space (CAS). The NACT within the two electronic states is computed using coupled-perturbed multi-configuration self-consistent field (CP-MCSCF) procedure implemented in MOLPRO quantum chemistry package.[62] The normal modes (Q_1 and Q_3) are first converted into a dimensionless form followed by transformation into plane polar coordinates (ρ and ϕ). The numerically calculated NACT (τ_ϕ^{12}) as shown in Figure 7a depicts one JT type seam passing through

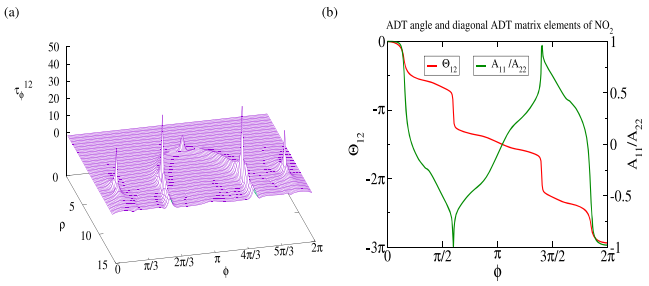

Figure 7. For $Q_1 - Q_3$ pair of NO_2 radical, (a) τ_ϕ^{12} over the plane of ρ and ϕ attains singular features along the semicircular JT type seam as well as in the RT regions. 1D functional variation of (b) ADT angle (Θ_{12}) and diagonal ADT matrix elements (A_{11}/A_{22}) are presented along ϕ coordinate at a fixed magnitude of ρ (= 10.9). Θ_{12} attains the value of 3π and A_{11}/A_{22} exhibits three sign inversions due to the JT and RT interactions.

the C_{2v} point with three prominent peaks—one at the C_{2v} point ($r_{NO_1} = r_{NO_2} = 1.213$ Å and $\angle ONO = 107.64°$) and the other two at C_s geometries ($r_{NO_1} = 0.805$ Å, $r_{NO_2} = 1.632$ Å and $\angle ONO = 109.2°$; and $r_{NO_1} = 1.632$ Å, $r_{NO_2} = 0.805$ Å and $\angle ONO = 109.2°$), whereas the RT interactions are observed at linear

https://dx.doi.org/10.1021/acs.jctc.9b00948
J. Chem. Theory Comput. 2020, 16, 1666−1680

geometries (r_{NO_1} = 1.129 Å and r_{NO_2} = 1.549 Å; and r_{NO_1} = 1.549 Å and r_{NO_2} = 1.129 Å).

The first principle based adiabatic PESs and NACT obtained from MOLPRO are plugged into the numeric section of "ADT" program to generate the ADT angles, ADT matrices and diabatic PESs. The differential equations are integrated along "Path 6" ranging from ρ = 0.0 to 14.0 and ϕ = 0 to 2π spanning 140 × 361 grid points. When the integration path forms a closed contour at ρ = 10.9, Figure 7b depicts ADT angle (Θ_{12}), which carries the signature of JT type CI seam and RT interaction by attending the magnitude of 3π. In Figure 7b, the diagonal elements of ADT matrix (A_{11}/A_{22}) validate the presence of JT type CI seam and RT interaction by undergoing three sign changes at the respective positions. Such ADT matrix can be employed to calculate diabatic PESs and diabatic couplings by performing a similarity transformation, where those can be found to be smooth, single-valued and continuous in the interested domain of nuclear CS (see Figure S4 of the Supporting Information).

6.3.2. H_3^+. H_3^+ is not only the simplest representative example of three center reactive system ($H + H_2^+$ or $H^+ + H_2$), but also it drew attention after its experimental detection by Oka[55] as a stable species. It involves several types of processes, like reactive charge transfer (RCT), reactive non charge transfer (RNCT) and nonreactive charge transfer (NRCT). Detailed calculation of diabatic surfaces has been carried out[33] with high level of accuracy and those surfaces have been used for extensive study of reactive scattering.[36] This system is selected to validate the program "ADT" for a three electronic state sub-Hilbert space.

Hyperspherical coordinate system is more advantageous for scanning adiabatic PESs as well as NACTs for triatomic reactive scattering processes. *Ab initio* quantities (adiabatic PESs as well as NACTs) are evaluated for lowest three singlet electronic states ($1^1A'$, $2^1A'$ and $3^1A'$) over the domain of nuclear CS constituting two hyperangles, namely, θ and ϕ for various fixed hyperradius ρ.[33] Calculation of adiabatic PESs is performed employing the CASSCF level of theory followed by internally contracted multireference configuration interaction (MRCI) calculation, whereas NACTs are computed using numerical finite difference method (DDR) implemented in MOLPRO.[62] We opted for Dunning's correlation consistent quintuple ζ (cc-pV5Z) basis set and CAS is chosen as 2 electrons in 10 orbitals. At and around ρ = 10 bohr, three equivalent semicircular accidental seams are observed, which are spreaded over θ greater than $\pi/3$ and ϕ ranging within 0 to $\pi/3$, $2\pi/3$ to π, and $4\pi/3$ to $5\pi/3$ between the two lowest electronic states.

At present, ADT is performed along "Path 1" in hyperspherical coordinates, where the hyperangles, θ and ϕ vary from 0 to $\pi/2$ and 0 to 2π, respectively spanning 89 × 180 grid points at several fixed magnitude of ρ. The differential equations are solved over a two-dimensional nuclear CS with appropriate relative and absolute error tolerances.[33] Figure 8a depicts one-dimensional (1D) functional forms of the Θ_{12} along ϕ grid at θ = 88° for various fixed magnitude of ρ (= 2.0, 4.0, 6.0, 8.0, 10.0, and 14.0 bohr) bearing the signature of "1−2" accidental seams at and around ρ = 10.0 bohr. Moreover, Figure 8b shows necessary sign inversions of the diagonal element of ADT matrix, A_{11} confirming the presence of "1−2" seams at the close vicinity of ρ = 10.0 bohr. This **A** matrix is used to construct the diabatic potential energy matrix (**W**) through similarity transformation of adiabatic PESs. Figures 9a and 9b depict the three adiabatic PESs and the corresponding diabatic PESs, respectively. For better view, the PESs are plotted only within the range ϕ = 90° to 210°. In Figure 9a, the ground and first excited adiabatic PESs ($1^1A'$ and $2^1A'$) show the CI seam passing through the C_{2v} point spread over C_s geometry clearly visible at θ = 90°, whereas in Figure 9b, those surfaces cross each other through the same seam.

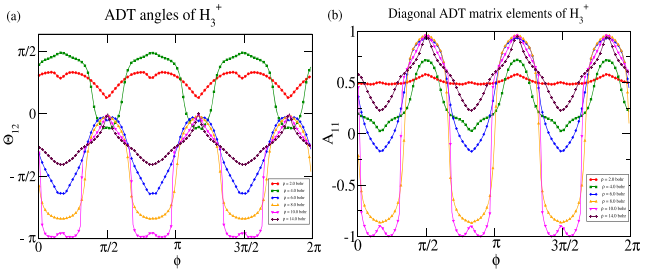

Figure 8. For H_3^+ species, (a) 1D cuts of Θ_{12} are plotted at θ = 88° for various fixed values of ρ (= 2.0, 4.0, 6.0, 8.0, 10.0, and 14.0 bohr). It can be clearly seen that Θ_{12} at ρ = 10.0 bohr carries the footprints of JT type accidental seams within "1−2" states. Similarly, (b) 1D curve of diagonal elements (A_{11}) are presented at the same θ value for several fixed magnitudes of ρ. At and around ρ = 10.0 bohr, A_{11} exhibits necessary number of sign flippings originated due to JT type accidental seams between ground and first excited electronic states.

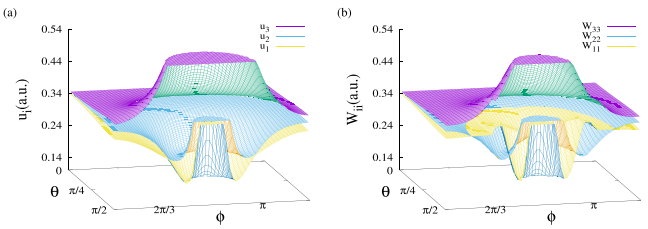

Figure 9. Adiabatic PESs of H_3^+, (a) u_1, u_2, and u_3 are presented over $\theta - \phi$ grid at ρ = 10.0 bohr. Similarly, the diabatic PESs, (b) W_{11}, W_{22}, and W_{33} are plotted over the same nuclear plane.

On the other hand, the D_{3h} CI between the first and second excited states ($2^1A'$ and $3^1A'$) is at θ = 0° both in adiabatic and diabatic PESs. In order to locate such a CI, Jacobi coordinates are employed to carry out 1D ADT calculation along a closed circular contour of radius q = 0.5 bohr centered around R, where r (H−H distance) = 2 bohr, R (distance of the center of closed contour from H−H) = 1.732 bohr, and γ (angle between r and R) = 90°. The *ab initio* adiabatic PECs and NACTs for low-lying three singlet electronic states are computed using the MRCI level of theory and CP-MCSCF methodology, respectively, using cc-pV5Z basis set with (2e, 11o) CAS. Subsequently, ADT equations are numerically integrated along the 1D grid of geometries containing 121 *ab initio* points from ϕ = 0 to 2π. Figure 10 clearly indicates the presence of one '2−3' CI encapsulated by the closed circular path, as Θ_{23} attains the magnitude of π at ϕ = 2π.

6.3.3. F + H_2. The elementary chemical reaction, F + H_2 has appeared to be interesting for decades due to its highly correlated electronic structure, significant spin−orbit coupling, and rich nonadiabatic interactions. While exploring the workability of our "ADT" algorithmic framework, we carry out an extensive study on the inherent nonadiabatic couplings among the low-lying three singlet electronic states ($1^2A'$, $1^2A''$ and $2^2A'$) of F+H_2 reactive system over the $\theta - \phi$ space for different fixed values of ρ in hyperspherical coordinates.[37,38]

At ρ = 10.0 bohr, adiabatic PESs as well as NACTs are computed employing MRCI level of methodology and analytic

https://dx.doi.org/10.1021/acs.jctc.9b00948
J. Chem. Theory Comput. 2020, 16, 1666−1680

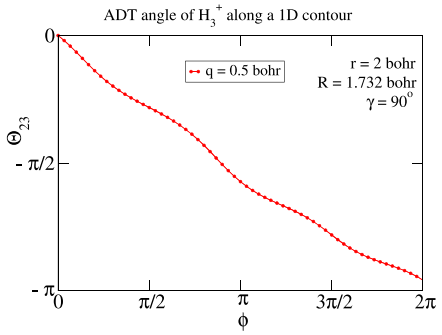

Figure 10. For H_3^+, the functional form of Θ_{23} is presented along a closed circular path (ϕ) at q = 0.5 bohr centered around R with r = 2 bohr, R = 1.732 bohr, and γ = 90°. The ADT angle (Θ_{23}) acquires the magnitude of π at $\phi = 2\pi$ validating the presence of '2−3" CI inside the contour.

gradient approach,[62] respectively, in order to carry out ADT to construct diabatic PESs. The electronic structure calculations are done in C_1 symmetry employing aug-cc-pVTZ basis set with seven (7) electrons distributed over eight (8) active orbitals.

We engage the first principle based BBO formalism as implemented in "ADT" software package to diabatize the adiabatic PESs and NACTs along "Path 6", where the hyperangles, θ and ϕ vary from 0 to $\pi/2$ and 0 to 2π, respectively, at a fixed value of ρ (= 10.0 bohr). Figure 11 depicts

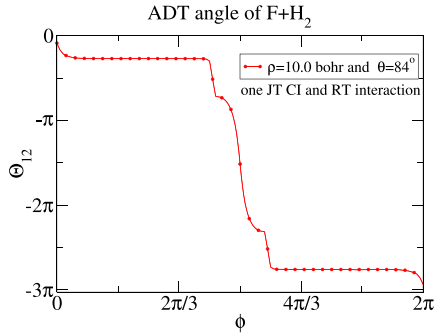

Figure 11. For F + H_2 collision process, 1D cut of Θ_{12} is plotted along ϕ coordinate at fixed values, ρ = 10.0 bohr and θ = 84°. The ADT angle acquires the magnitude of 3π depicting one JT CI and one RT interaction while quantization of "1−2" NACT along the closed circular contour.

that the resulting ADT angle (Θ_{12}) attains the magnitude of integral multiple of pi (3π) at the end of closing the contour due to one JT CI (π) between the two $^2A'$ states and one RT interaction (2π) corresponding to the $^2\Pi$ state.

6.3.4. NO_3 Radical. In the realm of nonadiabatic chemistry, NO_3 radical appears to be an excellent representative system for five coupled electronic states. Adhikari et al. have carried out thorough investigations to dig out its electronic structure and complex features of photoelectron spectra.[40] Low-lying five electronic states labeled as $\tilde{X}^2A_2'$ (1^2B_2), $\tilde{A}^2E''$(1^2A_2 and 1^2B_1) and $\tilde{B}^2E'$ (1^2A_1 and 2^2B_2) are mainly responsible for intense nonadiabatic interactions.[27,39] We deliberately pick up the degenerate components (Q_{3x} and Q_{3y}) of in-plane asymmetric stretching mode (ν_3) to depict the workability of our developed "ADT" software, since those modes are responsible for well-known electron nuclear coupling. CASSCF level of calculation is performed using 6-31g** basis set and (9e, 8o) CAS in C_1 symmetry to construct the adiabatic PESs. On the other hand, NACTs are calculated employing CP-MCSCF method implemented in MOLPRO quantum chemistry package.[62] Scanning of adiabatic PESs as well as NACTs is carried out using polar analogues (ρ and ϕ) of mass-weighted dimensionless normal mode coordinates (Q_{3x} and Q_{3y}). In NO_3 radical, strong JT interactions are observed within E'' and E' states at the D_{3h} point, whereas strong PJT effects are present within $\tilde{X}^2A_2'$ and $\tilde{B}^2E'$ states ("1−4" and "1−5" PJT couplings). On the other hand, three additional C_{2v} CIs are present at $\rho \approx 3.0$ and ϕ = 30°, 150°, 270° within "4−5" states. All of these nonadiabatic features increase the complexity of it is photoelectron spectra.

The coupled differential equations (see section S3 of the Supporting Information) are integrated over a two-dimensional grid of polar coordinates (ρ and ϕ) taking 50 × 180 *ab initio* points spanning from ρ = 0.0 to 5.0 and from ϕ = 0 to 2π. Here integration is performed along "Path 6" in which ADT angles are evaluated along a closed contour of ϕ for each negative step of integration from ρ = 5.0 to 0.0. As per the Cauchy's residue theorem, numerically calculated ADT angles turn into integer multiple of π or 0 if the enclosed functional form of NACTs do or do not exhibit characteristics of singularity. Figure 12a depicts

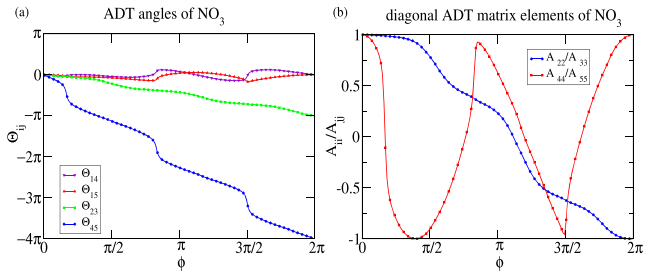

Figure 12. 1D cuts of (a) ADT angles of NO_3 radical for $Q_{3x} - Q_{3y}$ pairwise modes along ϕ coordinate for a definite ρ(= 4.9). Θ_{23} and Θ_{45} acquire the value of π and 4π due to one JT CI between "2−3" states and one JT along with three accidental CIs within "4−5" states, respectively. On the other hand, Θ_{14} and Θ_{15} attain the magnitude of zero (0) at the end of closing the contour though the intermediate values are nonzero. Similar to ADT angles, 1D plots of (b) A_{22}/A_{33} and A_{44}/A_{55} (at ρ = 4.9) also validate the CIs (JT as well as accidental) by undergoing the required number of sign changes (one and four, respectively).

one-dimensional plots of four ADT angles with the variation of ϕ coordinate at ρ = 4.9, where at $\phi = 2\pi$, Θ_{23}, and Θ_{45} attain the magnitude of π and 4π validating one "1−2" (JT) and four "4−5" (one JT and three accidental JT) CIs, respectively. On the contrary, Θ_{14} and Θ_{15} acquire the value of zero (0) though they have nonzero magnitude at intermediate ϕs. As a result, the diagonal elements of ADT matrix undergo sign flipping while encircling a conical intersection. Figure 12b shows one sign inversion for A_{22}/A_{33} due to one JT CI and four sign flippings for the A_{44}/A_{55} element originated due to one JT and three accidental CIs. Furthermore, diabatic potential energy matrix is evaluated by taking the similarity transformation of adiabatic potential energy matrix, where diabatic potentials as well as diabatic couplings appear to be smooth, single-valued and continuous functions (see Figure S5 of the Supporting Information).

6.3.5. $C_6H_6^+$ Radical Cation. $C_6H_6^+$ (Bz^+) radical cation can be considered as one of the representative cationic species in the domain of five electronic state BBO formalism due to its highly mysterious spectral features. In order to validate the superiority

https://dx.doi.org/10.1021/acs.jctc.9b00948
J. Chem. Theory Comput. 2020, 16, 1666−1680

of our developed code for a relatively larger cyclic hydrocarbon species, we selectively choose two degenerate components of asymmetric stretching mode, namely, Q_{16x} and Q_{16y} along which the low-lying five electronic states ($\tilde{X}^2E_{1g}$, $\tilde{B}^2E_{2g}$, and $\tilde{C}^2A_{2u}$) are strongly coupled with each other.[27] An extensive electronic structure calculation is carried out employing CASSCF level of methodology with 6-31g** basis set and (29e, 15o) CAS in C_1 symmetry to generate highly accurate adiabatic PESs. On the other hand, analytic NACTs are computed by employing the CP-MCSCF method.[62] It is important to note that the entire calculation is performed using polar counterparts (ρ and ϕ) of mass-weighted dimensionless normal mode coordinates (Q_{16x} and Q_{16y}). In Bz^+ radical cation, $\tilde{X}^2E_{1g}$ and $\tilde{B}^2E_{2g}$ exhibit severe JT distortion ("1−2" and "3−4" JT CI) at D_{6h} point, leading to lowering of symmetry in nuclear geometry. Nevertheless, Bz^+ does not exhibit any other accidental CI(s)/seam(s) or PJT interaction over the Q_{16x}−Q_{16y} nuclear plane.

With *ab initio* calculated adiabatic PESs and NACTs, coupled ADT equations (see section S3 of the Supporting Information) are numerically integrated over the 2D grid of geometries containing 20 × 180 (*ab initio*) points from ρ = 0.0 to 2.0 and ϕ = 0 to 2π. Similar to the case for the NO_3 radical, here also the differential equations are numerically integrated along "Path 6" to explore the quantization of NACTs along a closed contour. It is evident from Figure 13a that at ρ = 1.9, Θ_{12} and Θ_{34} acquire

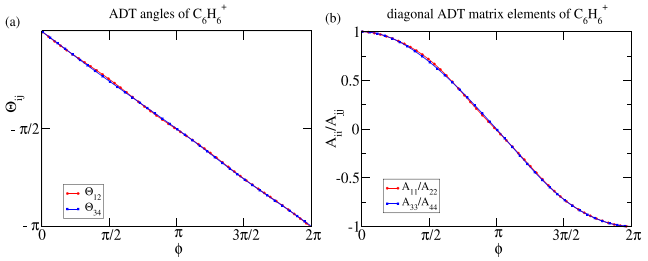

Figure 13. For $C_6H_6^+$ radical cation, 1D plots on (a) ADT angles along ϕ coordinate at a fixed magnitude of ρ (= 1.9). Θ_{12} and Θ_{34} attain the value of π at the end of closing the contour validating "1−2" and "3−4" JT CIs. (b) A_{11}/A_{22} and A_{33}/A_{44} at ρ = 1.9 also affirm "1−2" and "3−4" JT couplings by exhibiting sign inversions.

the magnitude of π at the end of the closed contour due to singular functional behavior of encapsulated "1−2" and "3−4" NACTs. The presence of these JT interactions are further validated by Figure 13b, which exhibits sign inversions of A_{11}/A_{22} and A_{33}/A_{44} at ρ = 1.9. It is noteworthy to mention that the diabatic potentials as well as couplings are found to be smooth, single-valued and continuous in the interested domain of nuclear CS (see Figure S6 of the Supporting Information).

6.3.6. 1,3,5-$C_6H_3F_3^+$ Radical Cation. We choose 1,3,5-$C_6H_3F_3^+$ ($TFBZ^+$) radical cation to depict the workability of BBO theory and, thereby, the validity of the "ADT" program for larger cyclic molecular systems containing six coupled electronic states is explored. Among the 30 normal modes of vibration, we selectively choose one pair, namely, C−C symmetric stretching (Q_{10x}−Q_{10y}) to establish our developed code for six state sub-Hilbert space. As the electronic states exhibit substantial JT stabilization while scanning the e' symmetric normal mode coordinates,[28,54] the Q_{10x}−Q_{10y} pair is stipulated to explore the JT as well as PJT interactions present in this radical cation. At the beginning, the ground state equilibrium geometry (D_{3h}) is optimized employing second order Møller−Plesset perturbation (MP2) level of theory with correlation-consistent polarized valence double-ξ (cc-pVDZ) basis set.

We scan adiabatic PESs for the low-lying six electronic states (denoted as $\tilde{X}^2E''$, $\tilde{A}^2A_2''$, $\tilde{B}^2E'$, and $\tilde{C}^2A_2'$) as a function of degenerate components of the mode (Q_{10}), keeping the other modes unaltered at their equilibrium. We employ CASSCF approach using cc-pVDZ basis set taking 11-electrons in 9-orbitals (11e, 9o) CAS comprising of 6048 configuration state functions (CSFs). The NACTs between the electronic states within this sub-Hilbert space (τ_x^{ij}, τ_y^{ij}, and τ_z^{ij}; $i, j = 1-6$; $i < j$) are calculated using CP-MCSCF method implemented in MOLPRO quantum chemistry software.[62] We are exploring diabatization of this radical cation using "ADT" to ensure the accuracy, efficiency as well as low memory requirement for six electronic state sub-Hilbert space.

The mass-weighted normal mode coordinates (Q_{10x}−Q_{10y}) are first converted to its dimensionless form and then, those are transformed into their polar analogues (ρ and ϕ). This pair is not only JT active but also those are responsible for more intense PJT interactions. The doubly degenerate electronic states, $\tilde{X}^2E''$ and $\tilde{B}^2E'$ undergo profound JT symmetry breaking phenomenon at D_{3h} geometry. Moreover, there are accidental CIs within $\tilde{B}^2E'$ state at $\rho \approx 0.34$ and ϕ = 60°, 180° and 300°. The corresponding ϕ components of NACTs (τ_ϕ^{12} and τ_ϕ^{45}) tend to become singular near the degenerate points. On the other hand, higher energy states ("4−6" and "5−6") exhibit strong PJT interactions, but low-lying "1−3" and "2−3" electronic states show subdued pseudo Jahn−Teller electron−nuclear coupling.

The *ab initio* calculated NACTs are incorporated in the "ADT" program and the corresponding differential equations are solved in the 2D grid of geometries over the ranges, ρ = 0 to 1.0 and ϕ = 0 to 2π containing 47 × 180 grid points. The integration is carried out employing "Path 6" implemented in "ADT". Figure 14a clearly reveals the position of one "1−2" JT

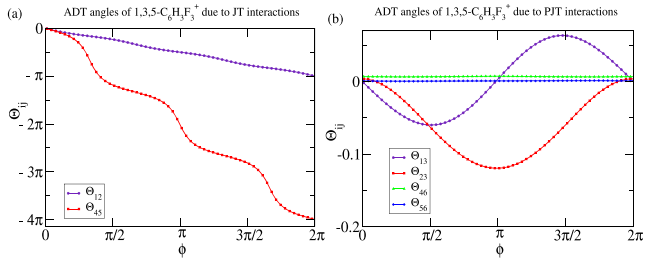

Figure 14. ADT angles of 1,3,5-$C_6H_3F_3^+$ radical cation for Q_{10x} − Q_{10y} normal mode pair along ϕ coordinate keeping the ρ value fixed at 0.96. (a) Θ_{12} and Θ_{45} acquire the magnitude of π and 4π representing one JT CI between "1−2" states and one JT along with three accidental CIs within "4−5" states, respectively, whereas the magnitude of (b) Θ_{13}, Θ_{23}, Θ_{46}, and Θ_{56} remains almost invariant at the end of closing the contour.

CI, one '4−5' JT CI and three '4−5' accidental CIs, as Θ_{12} and Θ_{45} attain the value of π and 4π, respectively. On the other hand, Figure 14b describes variation of ADT angles in case of PJT couplings (θ_{13}, θ_{23}, θ_{46} and θ_{56}), where the magnitude turns back to zero after the end of closing the contour though they have nonzero magnitudes in between. The diagonal elements of **A** matrix, A_{11}/A_{22} and A_{44}/A_{55} show required sign changes (Figure 15) bearing the indication of CIs within the closed contour. Finally, the calculation of diabatic surfaces and the coupling elements depict the efficiency as well as accuracy of our

https://dx.doi.org/10.1021/acs.jctc.9b00948
J. Chem. Theory Comput. 2020, 16, 1666−1680

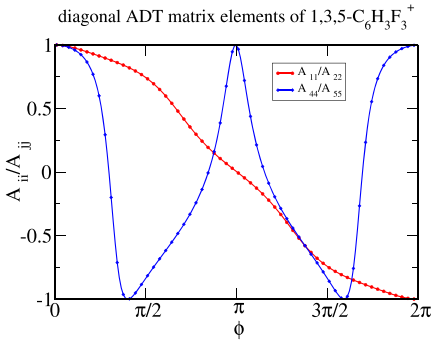

Figure 15. At ρ = 0.96, 1D plots of diagonal ADT matrix elements of 1,3,5- $C_6H_3F_3^+$ radical cation, namely, A_{11}/A_{22} and A_{44}/A_{55} confirm the presence of CIs (JT as well as accidental) by changing their sign once and four times, respectively.

developed code for higher dimensional sub-Hilbert spaces (see Figure S7 of the Supporting Information).

7. CONCLUSION

Accurate diabatization of adiabatic SE plays a major role in spectroscopic studies and reaction dynamics in order to include nonadiabatic interactions among several electronic states through multiple nuclear DOFs. In the perspective of nonadiabatic phenomena, BBO treatment based diabatization (ADT formalism) may be more accurate than the other contemporary ones, since both the inputs, adiabatic PESs and NACTs are *ab initio* calculated and ADT is theoretically and numerically "exact". According to BBO theory, adiabatic surfaces are diabatized considering a sub-Hilbert space of electronic states among which NACTs appear to be the key mechanistic elements due to their non-negligible magnitudes. Diabatization techniques from two to six electronic states sub-Hilbert spaces have already been shown as implemented ones.

Though the complexity and number of ADT equations increase with the increase of coupled electronic states, the newly implemented program framework can easily circumvent this difficulty while generating analytic expressions of ADT equations and calculating diabatic potential energy matrix elements numerically. One can directly supply the input files of adiabatic PESs and NACTs or can interface the molpro section of "ADT" to carry out *ab initio* electronic structure calculation for generating those input files and then, numeric section is employed for diabatization.

On the other hand, the challenges of BBO theory and ADT algorithm lies on the *ab initio* calculations, where it has to rely on good quality adiabatic PESs and accurate NACTs over a span of nuclear CS. Although one can invoke multireference methods like MRCI (for smaller sized molecules) or CASSCF (for relatively larger molecules) for calculating adiabatic PESs, accurate determination of NACTs is still very much an active area in the field of electronic structure theory. The present version of our "ADT" algorithm may also be employed to interface with direct dynamics (DD) approaches, namely, DD-vMCG and on-the-fly MCTDH, to efficiently solve the ADT equations for generating diabatic curves or surfaces. In summary, this programmatic framework will certainly be the first step to eliminate the bottleneck of implementing BBO formalism and to calculate diabatic PESs for higher dimensional sub-Hilbert spaces with multiple nuclear degrees of freedom.

■ ASSOCIATED CONTENT

Supporting Information

The Supporting Information is available free of charge at https://pubs.acs.org/doi/10.1021/acs.jctc.9b00948.

Source codes, license file, user_manual.pdf, and test_runs folder (ZIP)

ADT equations for three, four and five state sub-Hilbert space, description of components of the package, instructions for the users and diabatic PESs of NO_2, NO_3, $C_6H_6^+$ and 1,3,5-$C_6H_3F_3^+$ (PDF)

■ AUTHOR INFORMATION

Corresponding Author

Satrajit Adhikari − *School of Chemical Sciences, Indian Association for the Cultivation of Science, Kolkata 700032, India;* orcid.org/0000-0002-2462-4892; Email: pcsa@iacs.res.in

Authors

Koushik Naskar − *School of Chemical Sciences, Indian Association for the Cultivation of Science, Kolkata 700032, India*

Soumya Mukherjee − *School of Chemical Sciences, Indian Association for the Cultivation of Science, Kolkata 700032, India*

Bijit Mukherjee − *School of Chemical Sciences, Indian Association for the Cultivation of Science, Kolkata 700032, India*

Satyam Ravi − *School of Chemical Sciences, Indian Association for the Cultivation of Science, Kolkata 700032, India*

Saikat Mukherjee − *School of Chemical Sciences, Indian Association for the Cultivation of Science, Kolkata 700032, India*

Subhankar Sardar − *School of Chemical Sciences, Indian Association for the Cultivation of Science, Kolkata 700032, India; Department of Chemistry, Bhatter College, Dantan, Paschim Medinipur 721426, India*

Complete contact information is available at: https://pubs.acs.org/10.1021/acs.jctc.9b00948

Author Contributions

¶K.N. and So.M. contributed equally to this work.

Notes

The authors declare no competing financial interest.

■ ACKNOWLEDGMENTS

K.N. (File No.: 09/080(1068)/2018-EMR-I), So.M. (File No.: SPM-07/080(0250)/2016-EMR-I) and B.M. (File No.: 09/080(0960)/2014-EMR-I) thank CSIR India for providing research fellowships. S.R. and Sa.M. thank IACS for the same. S.S. is thankful to Principal, Bhatter College, Dantan, for providing the research facility in his institution. S.A. acknowledges DST, India, through Project No. EMR/2015/001314 for the research funding. Also thanks IACS for CRAY super computing facility.

■ REFERENCES

(1) Born, M.; Oppenheimer, J. R. On the Quantum Theory of Molecules. *Ann. Phys. (Berlin, Ger.)* **1927**, *389*, 457−484.

(2) Born, M.; Huang, K. *Dynamical Theory of Crystal Lattices*; Oxford University Press: Oxford, U.K., 1954.

(3) Hellmann, H. *Einfuhrang in die Quantenchemie*; Franz Duetiche: Leipzig, Germany, 1937.

(4) Feynman, R. Forces in Molecules. *Phys. Rev.* **1939**, *56*, 340−343.

(5) Top, Z. H.; Baer, M. Incorporation of Electronically Nonadiabatic Effects into Bimolecular Reactive Systems. I. Theory. *J. Chem. Phys.* **1977**, *66*, 1363−1371.
(6) Baer, M.; Niedner-Schatteburg, G.; Toennies, J. A Three Dimensional Quantum Mechanical Study of Vibrationally Resolved Charge Transfer Processes in H^++H_2 at E_{cm}=20 eV. *J. Chem. Phys.* **1989**, *91*, 4169−4182.
(7) Aguillon, F.; Sizun, M.; Sidis, V.; Billing, G. D.; Markovic, N. Semiclassical Coupled Wave Packet Study of the Nonadiabatic Collisions $Ar^+(J)$+H_2: Zero Angular Momentum Case. *J. Chem. Phys.* **1996**, *104*, 4530−4543.
(8) Baer, R.; Charutz, D.; Kosloff, R.; Baer, M. A Study of Conical Intersection Effects on Scattering Processes: The Validity of Adiabatic Single-Surface Approximations within a Quasi-Jahn-Teller Model. *J. Chem. Phys.* **1996**, *105*, 9141−9152.
(9) Adhikari, S.; Billing, G. D. The Conical Intersection Effects and Adiabatic Single-Surface Approximations on Scattering Processes: A Time-Dependent Wave Packet Approach. *J. Chem. Phys.* **1999**, *111*, 40−47.
(10) Baer, M.; Lin, S. H.; Alijah, A.; Adhikari, S.; Billing, G. D. Extended Approximated Born-Oppenheimer Equation. I. Theory. *Phys. Rev. A: At., Mol., Opt. Phys.* **2000**, *62*, 032506.
(11) Varandas, A. J. C.; Xu, Z. R. Nuclear Dynamics in the Vicinity of the Crossing Seam: Theory and Application to Vibrational Spectrum of H_3. *J. Chem. Phys.* **2000**, *112*, 2121−2127.
(12) Coe, J. D.; Martinez, T. J. Competitive Decay at Two- and Three-state Conical Intersections in Excited-State Intramolecular Proton Transfer. *J. Am. Chem. Soc.* **2005**, *127*, 4560−4561.
(13) Worth, G. A.; Robb, M. A.; Lasorne, B. Solving the Time-Dependent Schrödinger Equation for Nuclear Motion in One Step: Direct Dynamics of Non-Adiabatic Systems. *Mol. Phys.* **2008**, *106*, 2077−2091.
(14) Longuet-Higgins, H. C. Some Recent Developments in the Theory of Molecular Energy Levels. *Adv. Spectrosc.* **1961**, *2*, 429.
(15) Herzberg, G.; Longuet-Higgins, H. C. Intersection of Potential Energy Surfaces in Polyatomic Molecules. *Discuss. Faraday Soc.* **1963**, *35*, 77−82.
(16) Mead, C. A.; Truhlar, D. G. On the Determination of Born-Oppenheimer Nuclear Motion Wave Functions Including Complications due to Conical Intersections and Identical Nuclei. *J. Chem. Phys.* **1979**, *70*, 2284−2296.
(17) Hobey, W. D.; Mclachlan, A. D. Dynamical Jahn-Teller Effect in Hydrocarbon Radicals. *J. Chem. Phys.* **1960**, *33*, 1695−1703.
(18) Smith, F. T. Diabatic and Adiabatic Representations for Atomic Collision Problems. *Phys. Rev.* **1969**, *179*, 111−123.
(19) Baer, M. Adiabatic and Diabatic Representations for Atom-Molecule Collisions: Treatment of the Collinear Arrangement. *Chem. Phys. Lett.* **1975**, *35*, 112−118.
(20) Baer, M. Introduction to the Theory of Electronic Non-Adiabatic Coupling Terms in Molecular Systems. *Phys. Rep.* **2002**, *358*, 75−142.
(21) Baer, M. *Beyond Born - Oppenheimer: Conical Intersections and Electronic Nonadiabatic Coupling Terms*; Wiley Interscience: Hoboken, NJ, 2006.
(22) Baer, M.; Englman, R. A Study of the Diabatic Electronic Representation within the Born-Oppenheimer Approximation. *Mol. Phys.* **1992**, *75*, 293−303.
(23) Alijah, A.; Baer, M. The Electronic Adiabatic-Diabatic Transformation Matrix: A Theoretical and Numerical Study of a Three-State System. *J. Phys. Chem. A* **2000**, *104*, 389−396.
(24) Sarkar, B.; Adhikari, S. Extended Born-Oppenheimer Equation for a Three-State System. *J. Chem. Phys.* **2006**, *124*, 074101.
(25) Sarkar, B.; Adhikari, S. Curl Condition for a Four-State Born-Oppenheimer System Employing the Mathieu Equation. *J. Phys. Chem. A* **2008**, *112*, 9868−9885.
(26) Kumar Paul, A.; Sardar, S.; Sarkar, B.; Adhikari, S. Single Surface Beyond Born-Oppenheimer Equation for a Three-State Model Hamiltonian of Na_3 Cluster. *J. Chem. Phys.* **2009**, *131*, 124312.
(27) Mukherjee, S.; Mukherjee, B.; Adhikari, S. Five Electronic State Beyond Born-Oppenheimer Equations and Their Applications to Nitrate and Benzene Radical Cation. *J. Phys. Chem. A* **2017**, *121*, 6314−6326.
(28) Mukherjee, S.; Dutta, J.; Mukherjee, B.; Sardar, S.; Adhikari, S. Conical Intersections and Non-Adiabatic Coupling Terms in $C_6H_3F_3^+$: A Six State Beyond Born-Oppenheimer Treatment. *J. Chem. Phys.* **2019**, *150*, 064308.
(29) Mukherjee, B.; Naskar, K.; Mukherjee, S.; Ghosh, S.; Sahoo, T.; Adhikari, S. Beyond Born-Oppenheimer theory for spectroscopic and scattering processes. *Int. Rev. Phys. Chem.* **2019**, *38*, 287−341.
(30) Paul, A. K.; Ray, S.; Mukhopadhyay, D.; Adhikari, S. *Ab initio* Calculations on the Excited States of Na_3 Cluster to Explore Beyond Born-Oppenheimer Theories: Adiabatic to Diabatic Potential Energy Surfaces and Nuclear Dynamics. *J. Chem. Phys.* **2011**, *135*, 034107.
(31) Mukherjee, S.; Bandyopadhyay, S.; Paul, A. K.; Adhikari, S. Construction of Diabatic Hamiltonian Matrix from Ab Initio Calculated Molecular Symmetry Adapted Nonadiabatic Coupling Terms and Nuclear Dynamics for the Excited States of Na_3 Cluster. *J. Phys. Chem. A* **2013**, *117*, 3475−3495.
(32) Mukherjee, S.; Adhikari, S. The Excited States of K_3 Cluster: The Molecular Symmetry Adapted Non-Adiabatic Coupling Terms and Diabatic Hamiltonian Matrix. *Chem. Phys.* **2014**, *440*, 106−118.
(33) Mukherjee, S.; Mukhopadhyay, D.; Adhikari, S. Conical Intersections and Diabatic Potential Energy Surfaces for the Three Lowest Electronic Singlet States of H_3^+. *J. Chem. Phys.* **2014**, *141*, 204306.
(34) Mukherjee, S.; Mukherjee, B.; Sardar, S.; Adhikari, S. Ab Initio Constructed Diabatic Surfaces of NO_2 and the Photodetachment Spectra of its Anion. *J. Chem. Phys.* **2015**, *143*, 244307.
(35) Sardar, S.; Mukherjee, S.; Paul, A. K.; Adhikari, S. Conical Intersections Between X^2A_1 and A^2B_2 Electronic States of NO_2. *Chem. Phys.* **2013**, *416*, 11−20.
(36) Ghosh, S.; Mukherjee, S.; Mukherjee, B.; Mandal, S.; Sharma, R.; Chaudhury, P.; Adhikari, S. Beyond Born-Oppenheimer Theory for Ab Initio Constructed Diabatic Potential Energy Surfaces of Singlet H_3^+ to Study Reaction Dynamics Using Coupled 3D Time-Dependent Wave-Packet Approach. *J. Chem. Phys.* **2017**, *147*, 074105.
(37) Mukherjee, B.; Mukherjee, S.; Shamasundar, K. R.; Adhikari, S. Beyond Born-Oppenheimer Treatment for the Construction of Triple-Sheeted Accurate Diabatic Hamiltonian Matrix of F+H_2 System. *J. Phys.: Conf. Ser.* **2017**, *833*, 012004.
(38) Mukherjee, B.; Naskar, K.; Mukherjee, S.; Ravi, S.; Shamasundar, K. R.; Mukhopadhyay, D.; Adhikari, S. Conical Intersections and Diabatic Potential Energy Surfaces for the Three Lowest Electronic Singlet States of F+H_2 System. *J. Chem. Phys.* **2019**, to be submitted for publication.
(39) Mukherjee, B.; Mukherjee, S.; Sardar, S.; Shamasundar, K. R.; Adhikari, S. An Ab Initio Investigation of Non-Adiabatic Couplings and Conical Intersections Among the Lowest Five Electronic States of the NO_3 Radical. *Mol. Phys.* **2017**, *115*, 2833−2848.
(40) Mukherjee, B.; Naskar, K.; Mukherjee, S.; Shamasundar, K. R.; Adhikari, S. A Beyond Born-Oppenheimer Treatment of Five State Molecular System NO_3 and the Photodetachment Spectra of its Anion. *Chem. Phys.* **2018**, *515*, 350−359.
(41) Jackels, C. F.; Davidson, E. R. A Configuration Interaction Study of the Ground State Molecular Properties of NO_2. *J. Chem. Phys.* **1975**, *63*, 4672−4677.
(42) Kaldor, U. Symmetry Breaking in Radicals: NO_2, NS_2 and NO_3. *Chem. Phys. Lett.* **1991**, *185*, 131−135.
(43) Haller, E.; Köppel, H.; Cederbaum, L. S. The Visible Absorption Spectrum of NO_2: A Three-Mode Nuclear Dynamics Investigation. *J. Mol. Spectrosc.* **1985**, *111*, 377−397.
(44) Schinke, R.; Grebenshchikov, S. Y.; Zhu, H. The Photodissociation of NO_2 in the Second Absorption Band: Ab Initio and Quantum Dynamics Calculations. *Chem. Phys.* **2008**, *346*, 99−114.
(45) Joyeux, M.; Jost, R.; Lombardi, M. An Effective Model for the $X^2A_1 - A^2B_2$ Conical Intersection in NO_2. *J. Chem. Phys.* **2003**, *119*, 5923−5932.
(46) Sanrey, M.; Joyeux, M. Quantum Mechanical and Quasiclassical Investigations of the Time Domain Nonadiabatic Dynamics of NO_2

https://dx.doi.org/10.1021/acs.jctc.9b00948
J. Chem. Theory Comput. 2020, 16, 1666−1680

Close to the Bottom of the $X^2A_1 - A^2B_2$ Conical Intersection. *J. Chem. Phys.* **2006**, *125*, 014304.
(47) Weaver, A.; Metz, R. B.; Bradforth, S. E.; Neumark, D. M. Observation of the $\tilde{A}(^2B^2)$ and $\tilde{C}(^2A^2)$ states of NO_2 by negative ion photoelectron spectroscopy of NO_2^-. *J. Chem. Phys.* **1989**, *90*, 2070−2071.
(48) Weaver, A.; Arnold, D. W.; Bradforth, S. E.; Neumark, D. M. Examination of the $^2A_2'$ and $^2E'$ States of NO_3 by Ultraviolet Photoelectron Spectroscopy of NO_3^-. *J. Chem. Phys.* **1991**, *94*, 1740−1751.
(49) Eisfeld, W.; Morokuma, K. A Detailed Study on the Symmetry Breaking and its Effect on the Potential Surface of NO_3. *J. Chem. Phys.* **2000**, *113*, 5587−5597.
(50) Baltzer, P.; Karlsson, L.; Wannberg, B.; Öhrwall, G.; Holland, D. M. P.; MacDonald, M. A.; Hayes, M. A.; von Niessen, W. An Experimental and Theoretical Study of the Valence Shell Photoelectron Spectrum of the Benzene Molecule. *Chem. Phys.* **1997**, *224*, 95−119.
(51) Gilbert, R.; Sauvageau, P.; Sandorfy, C. Far-UV and Photoelectron Spectra of 1,3,5-Trifluorobenzene. *Chem. Phys. Lett.* **1972**, *17*, 465−470.
(52) Döscher, M.; Köppel, H.; Szalay, P. G. Multistate Vibronic Interactions in the Benzene Radical Cation. I. Electronic Structure Calculations. *J. Chem. Phys.* **2002**, *117*, 2645−2656.
(53) Köppel, H.; Cederbaum, L. S.; Domcke, W. Interplay of Jahn-Teller and Pseudo-Jahn-Teller Vibronic Dynamics in the Benzene Cation. *J. Chem. Phys.* **1988**, *89*, 2023−2040.
(54) Mondal, T.; Mahapatra, S. The Jahn-Teller and pseudo-Jahn-Teller effects in the low-lying electronic states of 1,3,5-trifluorobenzene radical cation. *Phys. Chem. Chem. Phys.* **2009**, *11*, 10867−10880.
(55) Oka, T. Observation of the Infrared Spectrum of H_3^+. *Phys. Rev. Lett.* **1980**, *45*, 531−534.
(56) Hartke, B.; Werner, H.-J. Time-dependent quantum simulations of FH_2^- photoelectron spectra on new ab initio potential energy surfaces for the anionic and the neutral species. *Chem. Phys. Lett.* **1997**, *280*, 430−438.
(57) Alexander, M. H.; Manolopoulos, D. E.; Werner, H.-J. An investigation of the F+H_2 reaction based on a full ab initio description of the open-shell character of the F(^{2}P) atom. *J. Chem. Phys.* **2000**, *113*, 11084−11100.
(58) Li, G.; Werner, H.-J.; Lique, F.; Alexander, M. H. New ab initio potential energy surfaces for the F + H_2 reaction. *J. Chem. Phys.* **2007**, *127*, 174302.
(59) Köppel, H.; Domcke, W.; Cederbaum, L. S. Multimode Molecular Dynamics Beyond the Born-Oppenheimer Approximation. *Adv. Chem. Phys.* **1984**, *57*, 59−246.
(60) Worth, G. A.; Cederbaum, L. S. BEYOND BORN-OPPENHEIMER: Molecular Dynamics Through a Conical Intersection. *Annu. Rev. Phys. Chem.* **2004**, *55*, 127−158.
(61) Ghosh, S.; Sahoo, T.; Adhikari, S.; Sharma, R.; Varandas, A. J. C. Coupled 3D Time-Dependent Wave-Packet Approach in Hyperspherical Coordinates: The D^++H_2 Reaction on the Triple-Sheeted DMBE Potential Energy Surface. *J. Phys. Chem. A* **2015**, *119*, 12392−12403.
(62) Werner, H.-J. et al. *MOLPRO*, version 2010.1, a package of ab initio programs. 2010; http://www.molpro.net.
(63) Thiel, A.; Köppel, H. Proposal and numerical test of a simple diabatization scheme. *J. Chem. Phys.* **1999**, *110*, 9371.
(64) Köppel, H.; Gronki, J.; Mahapatra, S. Construction scheme for regularized diabatic states. *J. Chem. Phys.* **2001**, *115*, 2377.
(65) Köppel, H.; Schubert, B. The concept of regularized diabatic states for a general conical intersection. *Mol. Phys.* **2006**, *104*, 1069.
(66) Mukherjee, S.; Mukherjee, B.; Dutta, J.; Sardar, S.; Adhikari, S. Topological Effects in Vibronically Coupled Degenerate Electronic States: A Case Study on Nitrate and Benzene Radical Cation. *ACS omega* **2018**, *3*, 12465−75.
(67) Worth, G. A.; Meyer, H.-D.; Köppel, H.; Cederbaum, L. S.; Burghardt, I. Using the MCTDH wavepacket propagation method to describe multimode non-adiabatic dynamics. *Int. Rev. Phys. Chem.* **2008**, *27*, 569.
(68) Richings, G. W.; Habershon, S. MCTDH on-the-fly: Efficient grid-based quantum dynamics without pre-computed potential energy surfaces. *J. Chem. Phys.* **2018**, *148*, 134116.
(69) Richings, G. W.; Polyak, I.; Spinlove, K.; Worth, G. A.; Burghardt, I.; Lasorne, B. Quantum dynamics simulations using Gaussian wavepackets: the vMCG method. *Int. Rev. Phys. Chem.* **2015**, *34*, 269.
(70) Richings, G. W.; Worth, G. A. A Practical diabatisation scheme for use with the direct-dynamics variational multi-configuration Gaussian method. *J. Phys. Chem. A* **2015**, *119*, 12457.
(71) Richings, G. W.; Worth, G. A. Multi-state non-adiabatic direct-dynamics on propagated diabatic potential energy surfaces. *Chem. Phys. Lett.* **2017**, *683*, 606.
(72) Baer, M. Electronic non-adiabatic transitions derivation of the general adiabatic-diabatic transformation matrix. *Mol. Phys.* **1980**, *40*, 1011.

https://dx.doi.org/10.1021/acs.jctc.9b00948
J. Chem. Theory Comput. 2020, 16, 1666−1680